Clim Dyn (2014) 43:553–574
DOI 10.1007/s00382-013-2034-z

Potential role of Atlantic Warm Pool-induced freshwater forcing in the Atlantic Meridional Overturning Circulation: ocean–sea ice model simulations

Liping Zhang · Chunzai Wang · Sang-Ki Lee

Received: 19 March 2013 / Accepted: 24 December 2013 / Published online: 7 January 2014
© Springer-Verlag Berlin Heidelberg 2014

Abstract Recent studies have indicated that the multidecadal variations of the Atlantic Warm Pool (AWP) can induce a significant freshwater change in the tropical North Atlantic Ocean. In this paper, the potential effect of the AWP-induced freshwater flux on the Atlantic Meridional Overturning Circulation (AMOC) is studied by performing a series of ocean–sea ice model experiments. Our model experiments demonstrate that ocean response to the anomalous AWP-induced freshwater flux is primarily dominated by the basin-scale gyre circulation adjustments with a time scale of about two decades. The positive (negative) freshwater anomaly leads to an anticyclonic (cyclonic) circulation overlapping the subtropical gyre. This strengthens (weakens) the Gulf Stream and the recirculation in the interior ocean, thus increases warm (cold) water advection to the north and decreases cold (warm) water advection to the south, producing an upper ocean temperature dipole in the midlatitude. As the freshwater (salty water) is advected to the North Atlantic deep convection region, the AMOC and its associated northward heat transport gradually decreases (increases), which in turn lead to an inter-hemispheric SST seesaw. In the equilibrium state, a comma-shaped SST anomaly pattern develops in the extratropical region, with the largest amplitude over the subpolar region and an extension along the east side of the basin and into the subtropical North Atlantic. Based on our model experiments, we argue that the multidecadal AWP-induced freshwater flux can affect the AMOC, which plays a negative feedback role that acts to recover the AMOC after it is weakened or strengthened. The sensitivity of AMOC response to the AWP-induced freshwater forcing amplitude is also examined and discussed.

Keywords Atlantic Warm Pool · Atlantic Meridional Overturning Circulation · Freshwater forcing

L. Zhang (✉) · S.-K. Lee
Cooperative Institute for Marine and Atmospheric Studies, University of Miami, Miami, FL, USA
e-mail: ocean.climate.ping@gmail.com

C. Wang · S.-K. Lee
NOAA Atlantic Oceanographic and Meteorological Laboratory, Miami, FL, USA

1 Introduction

The Atlantic Meridional Overturning Circulation (AMOC) is a system of surface and deep currents encompassing the entire Atlantic basin. It carries an enormous amount of heat northward (Ganachaud and Wunsch 2000), thereby altering climates in North America and Europe substantially. Previous studies suggested that the AMOC has large variations (e.g., te Raa and Dijkstra 2002; Lee and Wang 2010) and primarily varies on multidecadal timescales (e.g., Knight et al. 2005; Delworth and Mann 2000; Medhaug and Furevik 2011). It is also shown that the AMOC is a driving mechanism for the Atlantic Multidecadal Oscillation (AMO) (e.g., Delworth and Mann 2000; Knight et al. 2005; Dijkstra et al. 2006; Zhang et al. 2007), which is a climate mode wherein the North Atlantic sea surface temperature (SST) changes on the timescales of 30–80 years, with its largest variation centered in the high latitudes of the North Atlantic. The AMO variability is associated with changes in climate and extreme weather events such as rainfall and drought in North America and Atlantic hurricanes (e.g., Enfield et al. 2001; McCabe et al. 2004; Goldenberg et al. 2001; Bell and Chelliah 2006; Wang and Lee 2009; Wang et al. 2011). Thus, improving our understanding of the

AMOC is an important step for improving prediction of climate and Atlantic hurricane activity.

So far, there is no consensus for the physical mechanisms of the AMOC multidecadal fluctuations. Some studies argue that the AMOC variability is primarily an ocean mode with density fluctuations in the convection regions driven by advection of density anomalies from the low latitudes (e.g., Vellinga and Wu 2004; Krebs and Timmermann 2007a, b) or the northern high latitudes (e.g., Delworth et al. 1993). The AMOC is also deemed as a fully coupled atmosphere–ocean or atmosphere–sea ice-ocean mode with the deep water formation rate dominated by variations in the local wind forcing (e.g., Dickson et al. 1996; Häkkinen 1999; Eden and Willebrand 2001; Deshayes and Frankignoul 2008; Msadek and Frankignoul 2009; Medhaug et al. 2012). A common feature of the multidecadal variability in these models is that the AMOC responds to changes in upper-ocean density, caused by near-surface salinity changes over the North Atlantic sinking regions. This characteristic can also be seen from water-hosing experiments over the North Atlantic subpolar region (see a recent review by Clement and Peterson 2008). A freshening in the high latitude can lead to a weakening of the AMOC and subsequent impacts on the global climate through both oceanic bridge and atmospheric teleconnection (e.g., Manabe and Stouffer 1995, 1999a, b; Dong and Sutton 2002; Zhang and Delworth 2005; Timmermann et al. 2005; Wu et al. 2008; Okumura et al. 2009). However, different models differ in how these subpolar salinity anomalies recover: through modification of air–sea interaction over the midlatitude and subpolar North Atlantic, or by changes in oceanic salt transport from the low/high latitude.

It has been recently shown that the Atlantic Warm Pool (AWP)—a large body of warm water at the low latitude of the North Atlantic comprised of the Gulf of Mexico, the Caribbean Sea, and the western tropical North Atlantic (TNA) (Wang and Enfield 2001, 2003; Enfield and Lee 2005; Lee et al. 2007)—serves as an important gateway for air–sea feedbacks of heat, salt and moisture associated with the AMO (Wang et al. 2008b). The AWP multidecadal variability coincides with the signal of the AMO and the multidecadal TNA temperature fluctuations; that is, the warm (cool) phases of the AMO and warm (cool) TNA SST anomaly are characterized by repeated large (small) summer AWPs (Wang et al. 2008b). The NCAR community atmospheric model runs show that a large (small) AWP weakens (strengthens) the summer North Atlantic subtropical high and strengthens (weakens) the summer continental low over the North American monsoon region (Wang et al. 2008a). A large (small) AWP eventually results in an increased (decreased) freshwater (precipitation minus evaporation) and thus a decreased (increased) salinity in the tropical North Atlantic Ocean (Wang et al. 2013; Zhang and Wang 2012).

Based on the observational analyses of the AWP-induced freshwater and salinity budgets, Wang et al. (2013) hypothesized that the AWP variability may play a negative feedback role that acts to recover the AMOC after it is weakened or shut down. As the AMOC weakens, its northward heat transport reduces and thus the TNA cools (the AMO cold phase) and the AWP becomes small. A small AWP decreases rainfall in the TNA and increases the cross-Central American moisture export to the eastern North Pacific, both of which tend to increase salinity in the TNA Ocean. The AWP-induced freshwater flux and salinity anomaly are advected northward to the deep-water formation region and thus strengthens the AMOC. The purpose of the present paper is to test how the AWP-induced freshwater affect the AMOC via ocean pathways by performing numerical model experiments.

The AMOC's influence on the AMO, TNA temperature and thus the AWP has been studied in previous works (e.g., Zhang and Delworth 2005; Wang et al. 2008b; Wang and Zhang 2013). However, their associated low latitude freshwater feedback on the AMOC has not been broadly addressed. Although Kerbs and Timmermann (2007a, b) argue that during and after the Heinrich events, the ITCZ shift-induced precipitation can act as a recovery mechanism for the AMOC, it is not clear whether this recovery mechanism can exist at the multidecadal time scale. Moreover, the coupled model they used has a too coarse resolution to resolve various important components of the AMOC. In this paper, we focus on the effect of the AWP-induced freshwater flux on the AMOC at the multidecadal time scale. We attempt to address whether the AWP-induced freshwater flux has the potential to affect the AMOC. Although a lot of previous work studied on the role of freshwater in climate variability by using the ocean-only model (Huang and Mehta 2004, 2005; Huang et al. 2005) or the fully coupled models (e.g., Zhang and Busalacchi 2009; Zhang et al. 2011a, b, 2012, 2013; Zhang and Wu 2012), no study has previously focused on this AWP-induced freshwater and its effect on the AMOC. As far as we know, this is the first attempt to use an ocean–sea ice model to examine how the multidecadal AWP-induced freshwater variations affect the AMOC strength via the ocean pathways.

The paper is organized as follows. Section 2 briefly describes the ocean–sea ice model and experimental setup. The time evolution of AMOC index response to the AWP-induced freshwater change is shown in Sect. 3. Section 4 presents the ocean response when the AWP-induced freshwater change is increased by 3 times. Section 5 examines the sensitivity of ocean response to the AWP-induced freshwater forcing magnitude and sign. The discussion and summary are given in Sect. 6.

2 Model and experimental design

The global ocean–sea ice model, one of the components of NCAR Community Earth System Model version 1.0.4 (CESM1.0.4) (Danabasoglu et al. 2012), is used as a primary tool in this study. The ocean model is forced with the climatological Coordinated Ocean Sea-Ice Reference Experiment version 2 (CORE2) surface forcing dataset (Large and Yeager 2009). In the control simulation, the wind stress vector, shortwave radiative heat flux, downward longwave radiative heat flux and precipitation rate are specified, whereas the upward longwave radiative heat flux and turbulent surface fluxes are imposed interactively by using the wind speed, air temperature and specific humidity along with the model-produced SST. The control simulation starts with the January-mean climatological Polar Science Center Hydrographic Climatology potential temperature and salinity data and state of rest in the ocean model. The ocean model contains 60 vertical levels. Both the ocean and ice models have 320 longitudes and 384 latitudes on a displaced pole grid with a longitudinal resolution of about 1.0 degrees and a variable latitudinal resolution of approximately 0.3 degrees near the equator. Since the model is not coupled to the atmosphere and the heat flux change associated with the model-produced SST is relatively small, there is no significant air–sea feedback in this ocean–sea ice model as suggested by Danabasoglu et al. (2012). In this study, we use the default background vertical diffusive coefficient (0.16 cm^2/s), which produces a realistic AMOC strength at 26.5°N. With the climatological CORE2 forcing, the ocean–sea ice control simulation has been integrated for 1,500 years without apparent climate shifts. Figure 1a shows the AMOC index defined as the maximum overturning streamfunction at 26.5°N. To exclude or reduce surface wind driven overturning, we further use a criterion that the maximum streamfunction should be located deeper than 500-m. After 800 years, the AMOC becomes stable with a magnitude of about 16.8 Sv, which is in the observed range of 14–20 Sv (Kanzow et al. 2010). The AMOC's spatial structure simulated by the CESM1.0.4 ocean–sea ice model (averaged between years 1,000 and 1,500) reasonably captures the mean state of the AMOC derived from observations (e.g., Lumpkin and Speer 2007), with an anticyclonic cell (AMOC) in the upper 2,800 m and a cyclonic cell (Antarctic Bottom Water, AABW) in the deep ocean (Fig. 1b).

Figure 2 shows the detrended annual mean AWP, TNA SST and AMO indexes from the extended reconstructed sea surface temperature (ERSST) data (Smith et al. 2008). As expected, three indexes are closely linked with each other, with almost the same phase both on interannual and multidecadal timescales. Here, we are more interested in the multidecadal AWP (TNA or AMO) variability, since

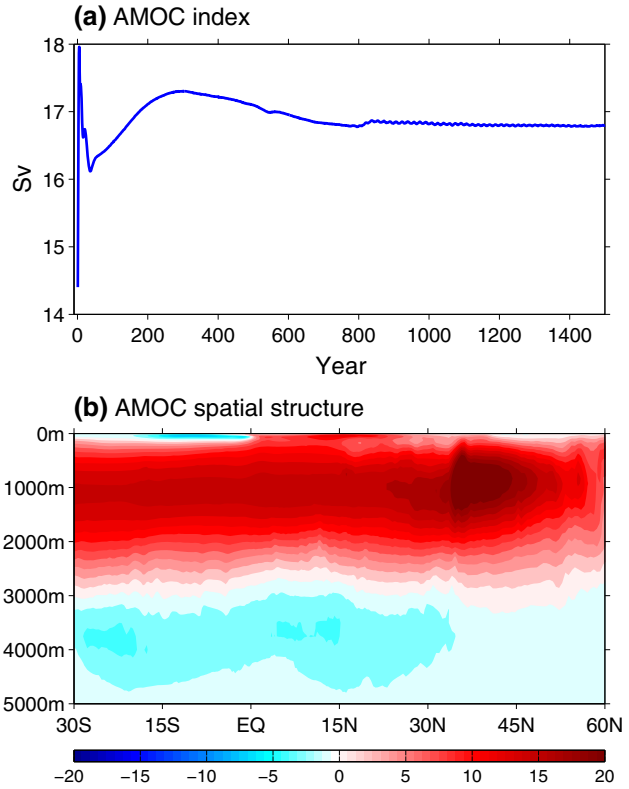

Fig. 1 AMOC variations in control simulation. **a** AMOC index (maximum overturning streamfunction blew 500-m and at 26.5°N). **b** Time-averaged AMOC spatial structure during year 1,000–1,500. Unit is Sv

the low latitude freshwater needs enough time to be transported to the deep convection region and then have the potential to affect the AMOC. As shown in Fig. 3a, the TNA region experiences an excess of freshwater [negative evaporation minus precipitation (EmP) anomaly] in summer during large AWPs and vice versa for small AWPs (Fig. 3b). Here, the EmP anomaly is from the twentieth century Reanalysis (20CRv2) data (Compo et al. 2011). The maximum freshwater change mainly occurs in the eastern TNA Ocean, with a magnitude up to 0.8 mm/day. These TNA EmP anomalies are equivalent to a net freshwater change of about 0.1 Sv. The freshwater change is primarily attributed to the AWP-induced precipitation variations, while the evaporation is of secondary importance (Wang et al. 2013). Similar results can be obtained during the different phases of the AMO and multidecadal TNA temperature fluctuations, albeit with a slight amplitude difference (Fig. 3c–f). To examine whether the multidecadal low latitude freshwater change can affect the AMOC, we impose a freshwater flux forcing in the ocean–sea ice model, which has the same pattern as the observed EmP pattern (Fig. 3a, b) but only with the negative (positive) EmP anomalies over the TNA region (5°N–30°N, coast to coast) during the multidecadal large (small) AWP

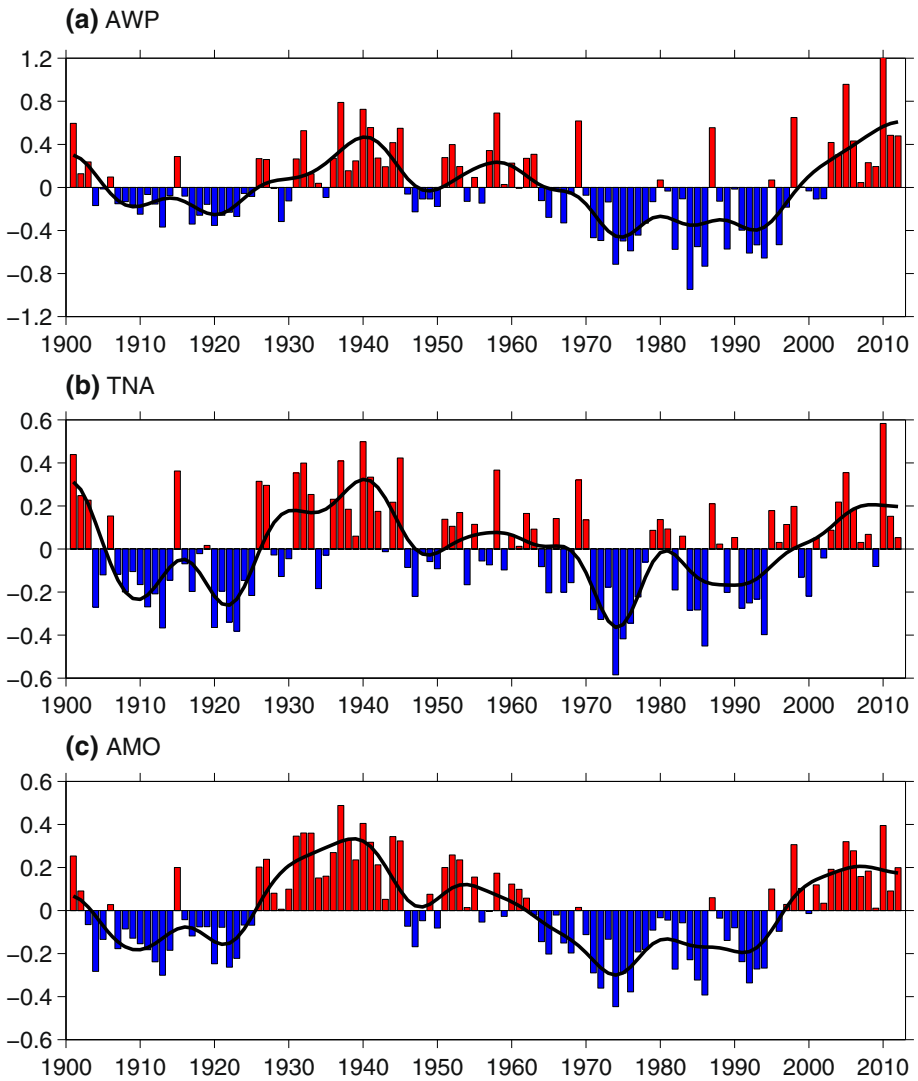

Fig. 2 Shown are the detrended (removing the linear trend) annual mean **a** AWP area anomaly indices (100 %), **b** TNA SST anomaly indices (°C) and **c** AMO indices (°C) from ERSST data (Smith et al. 2008). The AWP area index is calculated as the area of SST warmer than 28.5 °C divided by the long term mean AWP area. The TNA SST index is calculated as the area averaged SST from 5°N to 25°N and from Atlantic east coast to west coast. The AMO index is defined as the detrended area averaged SST from 0°N to 60°N and from Atlantic east coast to west coast. The *black lines* imposed on **a**–**c** are the multidecadal AWP, TNA and AMO indexes, which are filtered by an 11-year low pass filter

periods. Similar experiments are conducted for the warm and cool phases of the AMO and TNA temperature variations. It is found that the ocean responses share great similarities under the AMO-, TNA temperature- and AWP-induced freshwater forcing (not shown). Therefore, we only use the ocean responses associated with the AWP in this study. To avoid potential numerical instability, the imposed forcing is gradually reduced to zero within 5° inward from both zonal and meridional boundary. To increase the signal-to-noise ratio, the magnitudes of the imposed forcing are amplified by a factor of three in both the large and small AWP experiments.

The sensitivity of the coupled ocean–sea ice response to the forcing amplitudes and sign will be also assessed by conducting 4 additional experiments with the large and small AWP-induced freshwater change amplified by factors of five and one. It should be noted that in the ocean–sea ice model, the anomalous EmP forcing is only applied to the precipitation, with the other climatological forcing unchanged. Overall, we conduct 6 forced experiments, with 3 different freshwater forcing magnitudes (amplified fivefold, threefold and one fold) for both the multidecadal large and small AWPs. Each experiment starts from the 1300th year of the long control simulation and integrates for 150 years. The difference between these forced experiments and the control simulation is taken as the response. These experiments are named as $5AWP^{+}$, $5AWP^{-}$, $3AWP^{+}$, $3AWP^{-}$, $1AWP^{+}$, and $1AWP^{-}$.

Note that the freshwater is not exactly antisymmetric during large and small AWPs. The same is true for the different phases of the TNA temperature and AMO. Therefore, we cannot exactly assess whether the ocean response is linear or not by using the realistic freshwater forcing. To address this issue, we conduct a series of idealized freshwater experiments. As displayed in Fig. 3g, h, we impose an idealized freshwater forcing over the TNA, which has the maximum value in the center and decreases toward the meridional boundaries using a sine function.

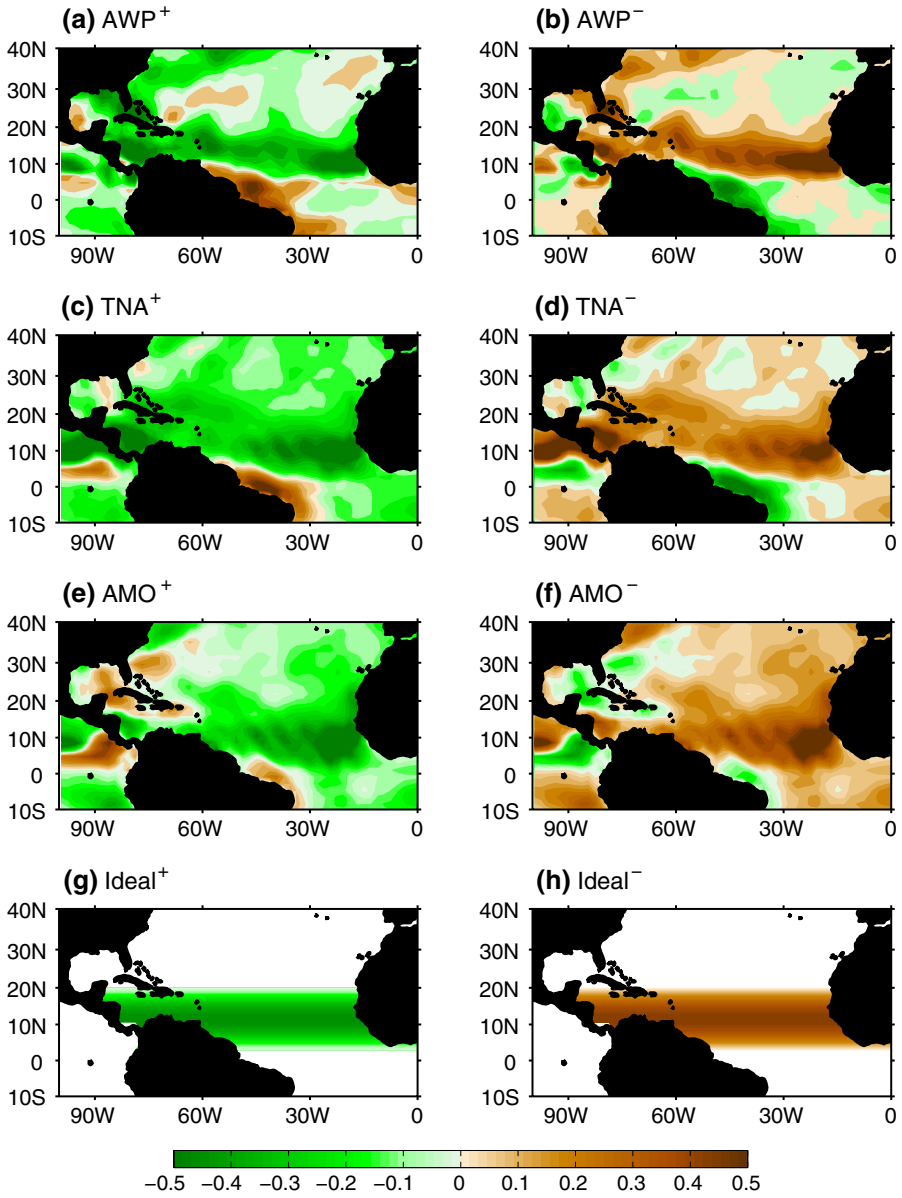

Fig. 3 Composites of the annual EmP anomalies (mm/day) on multidecadal timescales. Shown are for the positive and negative phases of the AWP size (**a**, **b**), TNA SST anomalies (**c**, **d**), and AMO (**e**, **f**) from the datasets of 20CRv2 (Compo et al. 2011). **g**, **h** show the idealized positive and negative freshwater forcing. Using the multidecadal AWP index, we identify the positive (negative) phase of the AWP as AWP^{+} (AWP^{-}) by a warm pool 10 % larger (smaller) than the long term mean. We identify the positive (negative) phase of the TNA as TNA^{+} (TNA^{-}) by a SST 10 % warmer (cooler) than the long term mean. The same 10 % criterion is used for the AMO index

The integrated freshwater amount in the positive phase of the idealized experiment (Fig. 3g) equals to the realistic freshwater amount averaged among three different indices (Fig. 3a, c, e). This guarantees that the idealized annual mean freshwater input to the ocean represents realistic annual mean low latitude freshwater forcing. By multiplying −1 to the positive phase of the freshwater anomaly, we obtain the negative phase of freshwater in the idealized experiment (Fig. 3h). Thus, the positive and negative phases of the freshwater over the TNA are exactly anti-symmetric. Similarly, we perform 6 experiments with the positive and negative idealized freshwater changes amplified by factors of five, three and one. These experiments are named as $5Ideal^{+}$, $5Ideal^{-}$, $3Ideal^{+}$, $3Ideal^{-}$, $1Ideal^{+}$, and $1Ideal^{-}$, respectively.

3 Time evolution of the AMOC response to the AWP-induced freshwater

We first show the time evolution of AMOC index response to the different magnitudes of freshwater forcing in the TNA region, as displayed in Fig. 4. Here, the AMOC index is defined as the maximum streamfunction below 500 m and in a latitude band between 20°N and 60°N. It is seen that the AMOC decreases (increases) in response to a large (small) AWP-induced freshwater change (Fig. 4), consistent with our main hypothesis. Furthermore, the more (less) freshwater flux occurs in the TNA region, the larger decrease (increase) of AMOC amplitude appears. With the large AWP-induced freshwater forcing amplified fivefold, the AMOC decrease can be as large as 8 Sv. When the

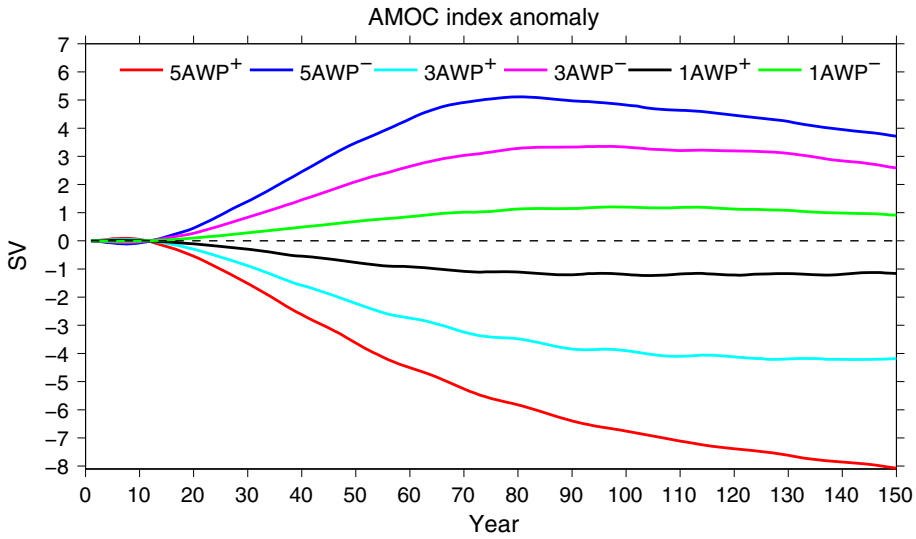

Fig. 4 Time evolution of the AMOC index for 6 experiments forced by the large and small AWP-induced freshwater forcing amplified fivefold (*red* and *dark blue lines*), threefold (*light blue* and *pink lines*) and one fold (*black* and *green lines*), respectively

amplified factor of freshwater forcing decreases to three and one, the corresponding AMOC index decreases by 4 and 1 Sv, respectively. On the contrary, the AMOC index increases by 1, 2.8 and 3.8 Sv, when we impose a small AWP-induced freshwater with an amplified factor equals to one, three and five, respectively. These results support our hypothesis that the AWP-induced freshwater has the potential to affect the AMOC and may act as a negative feedback to recover the AMOC. Given the different magnitude responses of the AMOC to the freshwater forcing, we will first show the ocean response in $3AWP^+$ run as an example in Sect. 4 and then examine the sensitivity of ocean response to the low latitude freshwater forcing magnitude and sign in Sect. 5.

Further examination finds that the AMOC exhibits negligible changes in the first 20 years for all runs (Fig. 4). After 20 years, the AMOC index gradually decreases or increases. After about the 30th year, the AMOC change becomes significant. This indicates that two decades is the delay time for the AWP-induced freshwater forcing to influence the AMOC strength. This delayed time for the AMOC response is expected to relate with the ocean circulation advection time. Therefore, in Sect. 4, we will show the ocean spin up response (first 40 years) and the relative equilibrium state (100–150 years).

4 Ocean response in $3AWP^+$ run

4.1 Spin up process

4.1.1 Sea surface salinity response

We first examine the spin up response by focusing on the first 40-years of the 150-year model integration. With the positive PmE forcing in the AWP region, the direct response in the first year is a significant decrease of sea surface salinity (SSS) in the vicinity of the forcing region (Fig. 5a), with a maximum reaching 0.3PSU. Associated with the salinity decrease, the mixed layer depth becomes shallow accordingly. In the second year, the SSS gradually decreases and spreads northeastward due to the advection of the Gulf Stream (Fig. 5b). At the meantime, the mixed layer depth shoals northeastward. In the third to fifth years, the negative SSS anomaly is continually advected to the north and the corresponding mixed layer depth decrease also extends to the north (Fig. 5c, d). After about the tenth year, the salinity anomaly can reach the east Greenland Irminger Sea where the deep convection forms (Pickart et al. 2002) (Fig. 5e). At this moment, the mixed layer depth is decreased in the Irminger Sea. In the fifteenth year and afterward (Fig. 5f), the salinity further spreads to the Labrador Sea, which is another deep convection region (Lavender et al. 2002), and then advected southward to the Gulf Stream region by the Labrador Current. The entire subpolar basin is occupied with the negative SSS anomalies after the 20th year (Fig. 5g–i). Accordingly, the mixed layer depth continually shallows in the deep convection region and further extends to the entire subpolar region. On the other hand, the salinity anomaly in the midlatitude also advected eastward by the North Atlantic Current (NAC). Then, the SSS anomaly is advected southeastward to the tropics by the Canary current and eventually advected back to the AWP region (Fig. 5e–g). Therefore, the almost entire Northern Atlantic Ocean experiences a negative SSS anomaly and a decrease of the mixed layer depth after about the 20th year. Obviously, the subpolar gyre and subtropical gyre play an important role in spreading the salinity anomaly from the low latitude to the other regions. Note that significant salinity and mixed layer depth

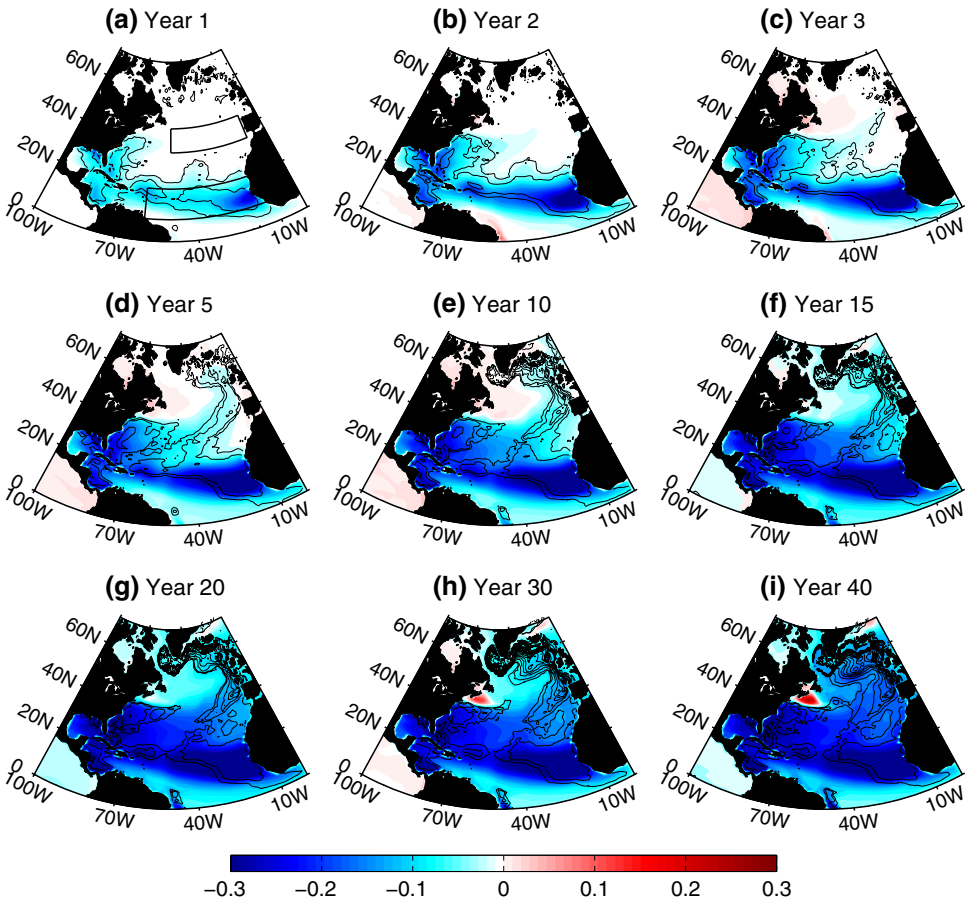

Fig. 5 Time evolution of sea surface salinity (PSU) response in 3AWP^{+} run in the first 40 years. The *black boxes* in **a** denote the regions performing the time-integrated salt budget in Fig. 6. The *black contour* imposed on salinity is the mixed layer depth response (contour interval is −2 m). Here, the mixed layer depth is defined as the depth where the difference with the potential density at the first layer equals to 0.125 kg/m^3

anomalies in the Irminger and Labrador Seas appear about 20 years later, which coincides with the delayed time for the AMOC response exhibited in Fig. 4. This suggests that the deep convection regions act as a switch for the AMOC response to the AWP-induced freshwater forcing.

To further confirm the contribution of current advection to the salinity spreading, we perform a time-integrated mixed layer salt budget in the eastern mid-latitude and TNA oceans (see two boxes in Fig. 5a). The salt equation is as follow:

$$\int_0^t \frac{\partial S}{\partial t} dt = -\int_0^t \left(u\frac{\partial S}{\partial x} + v\frac{\partial S}{\partial y} + w\frac{\partial S}{\partial z} \right) dt + \int_0^t Mix dt \quad (1)$$

$$Mix = \partial_{zz} S + S_{KPP} + S_0(E - P - R)/H$$

These terms are salinity changes induced by, from left to right, local change, oceanic advection, and mixing term. Here, the mixing term includes vertical diffusions, nonlocal diffusion due to K-Profile Parameterization (KPP) mixing and surface freshwater source. The salinity equation is integrated in the mixed layer. Here, we choose the mixed layer depth as a constant (50 m). As shown in Fig. 6a, the negative salinity anomaly in the eastern midlatitude ocean is primarily attributed to the advection and countered by the mixing term. This suggests that the vertical diffusion acts to dilute the upper ocean salinity anomalies down to the deep ocean and thus decreases the salinity anomaly in the surface mixed layer. Further decomposition of the advection finds that the advection contribution is mainly associated with the salinity anomaly advection by the mean zonal current, while the salinity anomaly advection by the mean meridional current is of secondary importance (Fig. 6b). The mean salinity advection by the anomalous meridional current tends to reduce the negative salinity anomaly and thus plays a damping role, indicating that there is an anomalous northward current, which will be seen in Figs. 8, 9. The remaining terms play a negligible role in salinity anomaly (Fig. 6b). This salt budget analysis suggests that the midlatitude salinity anomaly is largely due to the salinity advection by the mean circulation. In contrast, the salinity change in the TNA forcing region is dominated by the mixing term predominantly by the direct freshwater forcing imposed, whereas the advection term contributes negatively (Fig. 6c). The damping role of advection mainly arises from the advection by the mean current, particularly the mean meridional current (Fig. 6d). The mean meridional and zonal flows tend to advect the salinity anomaly off the TNA region. The mean salinity

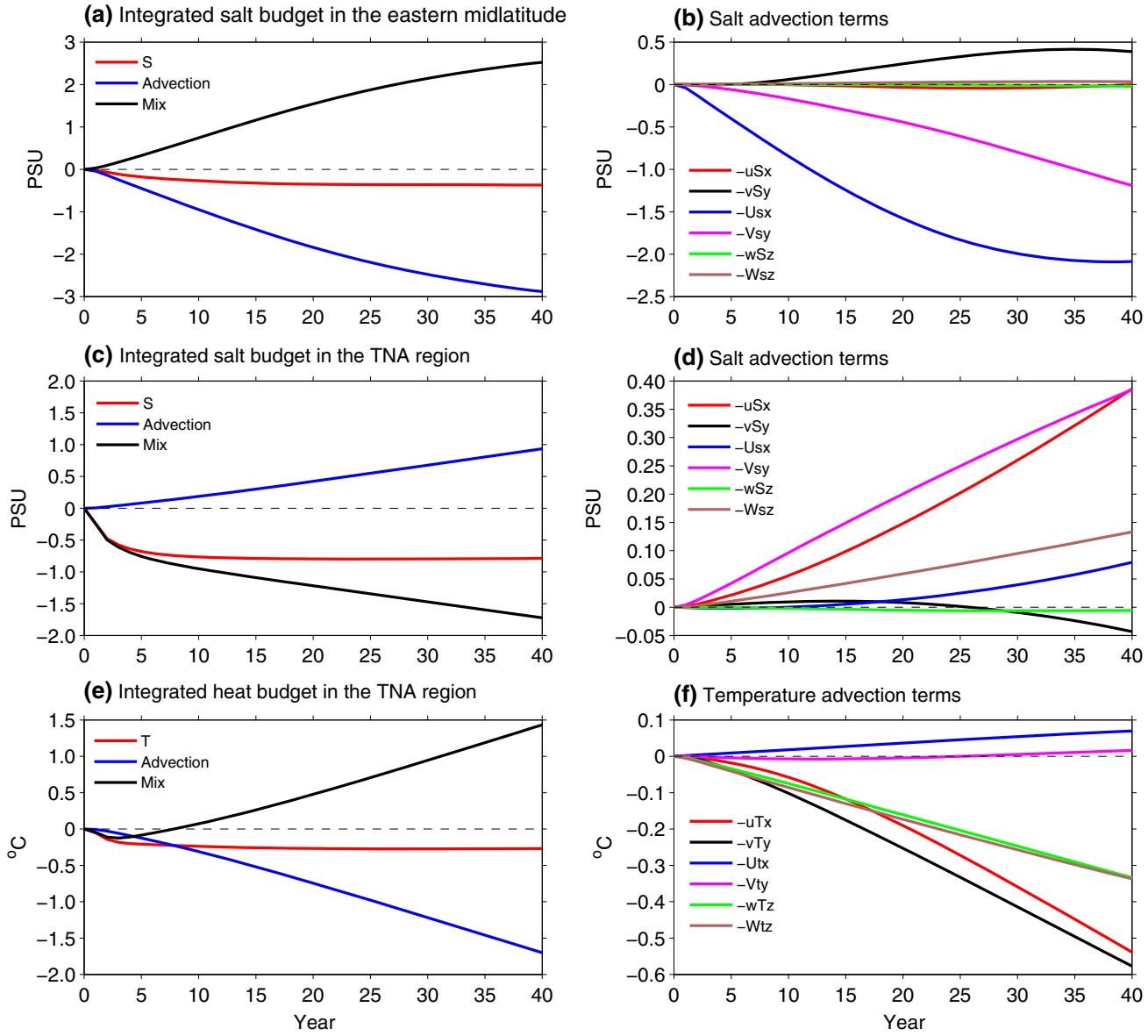

Fig. 6 Time-integrated salinity (PSU) budget in the **a** eastern midlatitude and **c** TNA regions (see *black boxes* in Fig. 5a) in 3AWP^{+} run. **b** and **d** depict the different terms of salt advection. The *capital* and *lower case letters* denote mean and anomaly. −uSx, −vSy, −Usx, −Vsy, −wSz and −Wsz represent term $-U'\partial\overline{S}/\partial x$, $-V'\partial\overline{S}/\partial y$, $-\overline{U}\partial S'/\partial x$, $-\overline{V}\partial S'/\partial y$, $-W'\partial\overline{S}/\partial z$and $-\overline{W}\partial S'/\partial z$, respectively. **e**, **f** Is the same as **c**, **d** but for the time-integrated temperature (°C) budget in the TNA region

advection by the anomalous zonal current also contributes to the damping effect, implying that an anomalous westward current is generated over the TNA region, which will be discussed in Sect. 4.1.2.

4.1.2 Sea surface height and surface current response

Associated with a decrease in surface salinity, the sea surface height (SSH) increases accordingly (Fig. 7), with a maximum increase co-located with the center of the maximum decrease of surface salinity. It is found that the ocean spin up process manifested in SSH is well correlated with SSS (Figs. 5 vs. 7), with the same spatial structure but with the opposite sign. In the first year, the SSH anomaly is mainly trapped in the TNA region (Fig. 7a). In the following years, the SSH anomalies are extended to the Gulf Stream and its downstream regions (Fig. 7b, c), and are further spread to the entire subpolar gyre and subtropical gyre region (Fig. 7d–i). These originate from the fact that a decrease of salinity leads to a decrease of density, an expansion of surface water volume for given mass, and thus an increase of the SSH. The SSH response to the freshwater anomalies is consistent with previous water-hosing experiments (e.g., Stouffer et al. 2007; Zhang et al. 2011a, b).

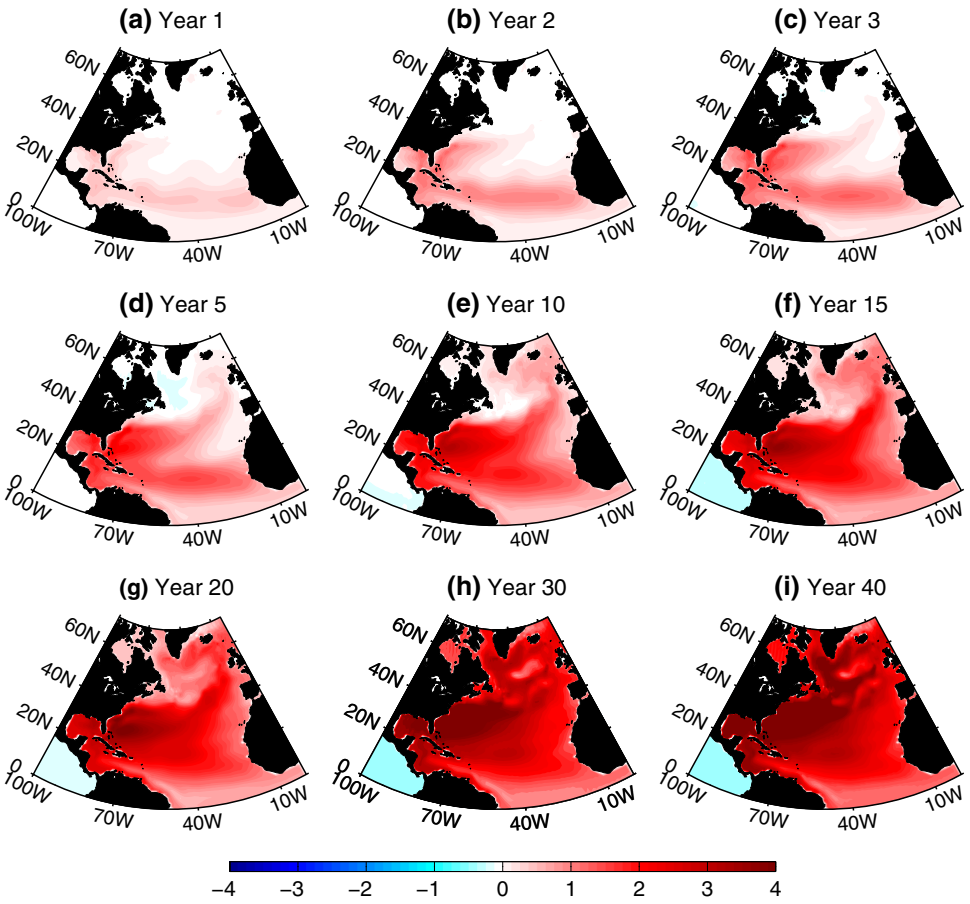

Fig. 7 Time evolution of sea surface height (cm) response in $3AWP^{+}$ run in the first 40 years

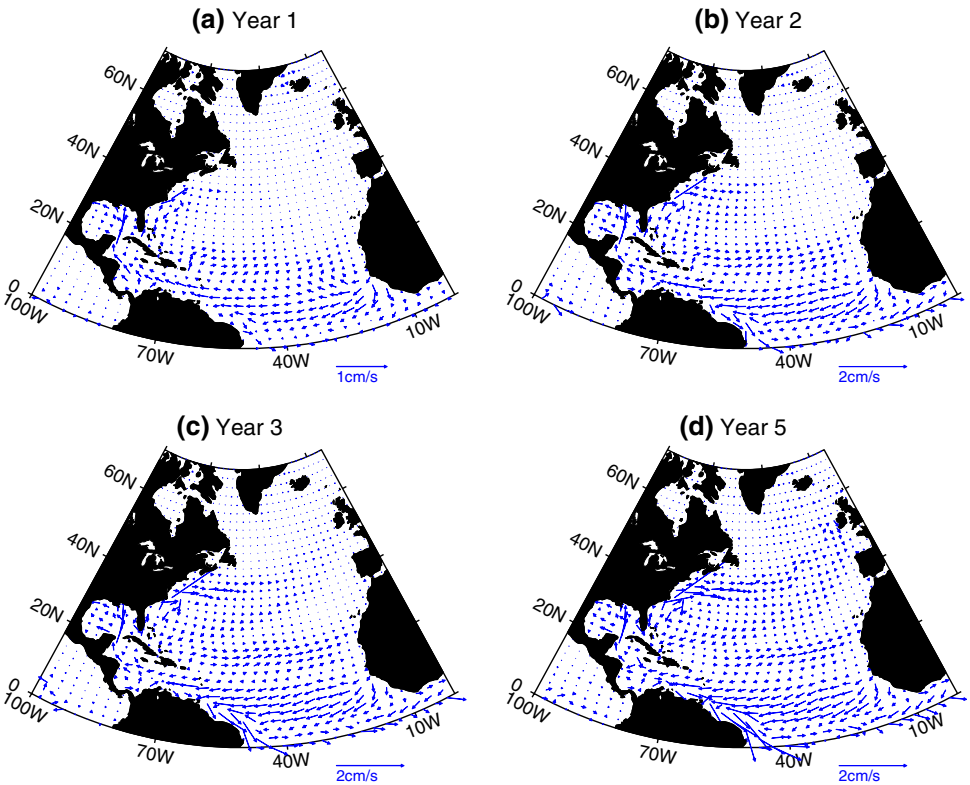

Fig. 8 Time evolution of surface horizontal current (averaged in the *upper* 50 m; cm/s) in $3AWP^{+}$ run in the first 5 years

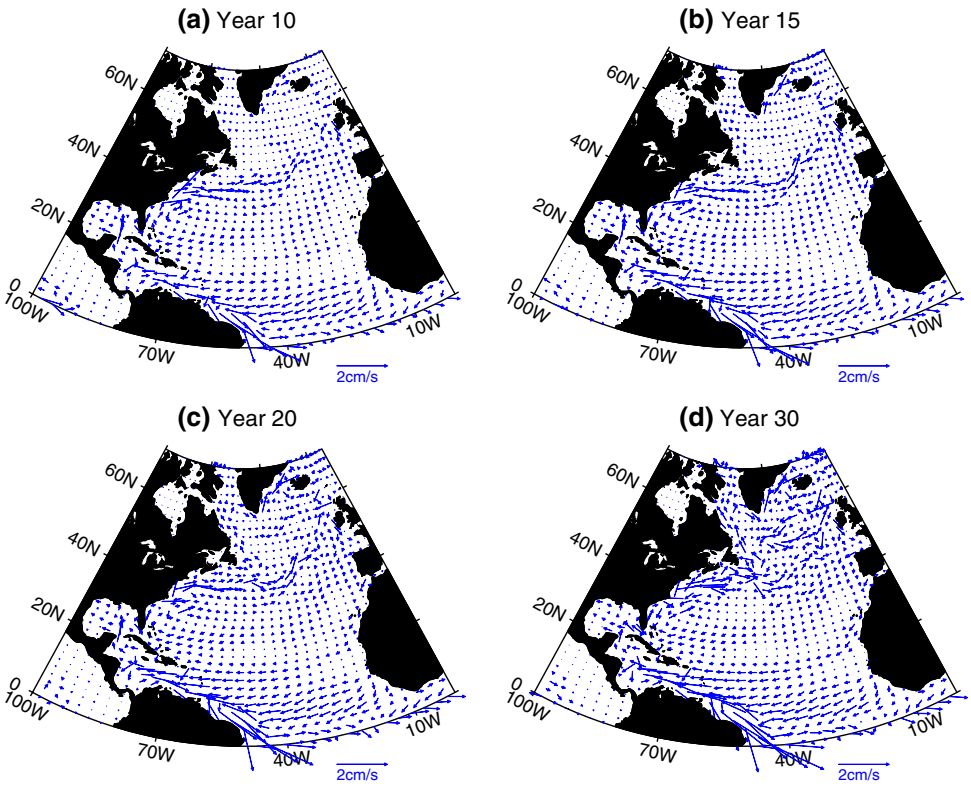

Fig. 9 Time evolution of surface horizontal current (averaged in the *upper* 50 m; cm/s) in 3AWP^{+} run in the first 10–30 years

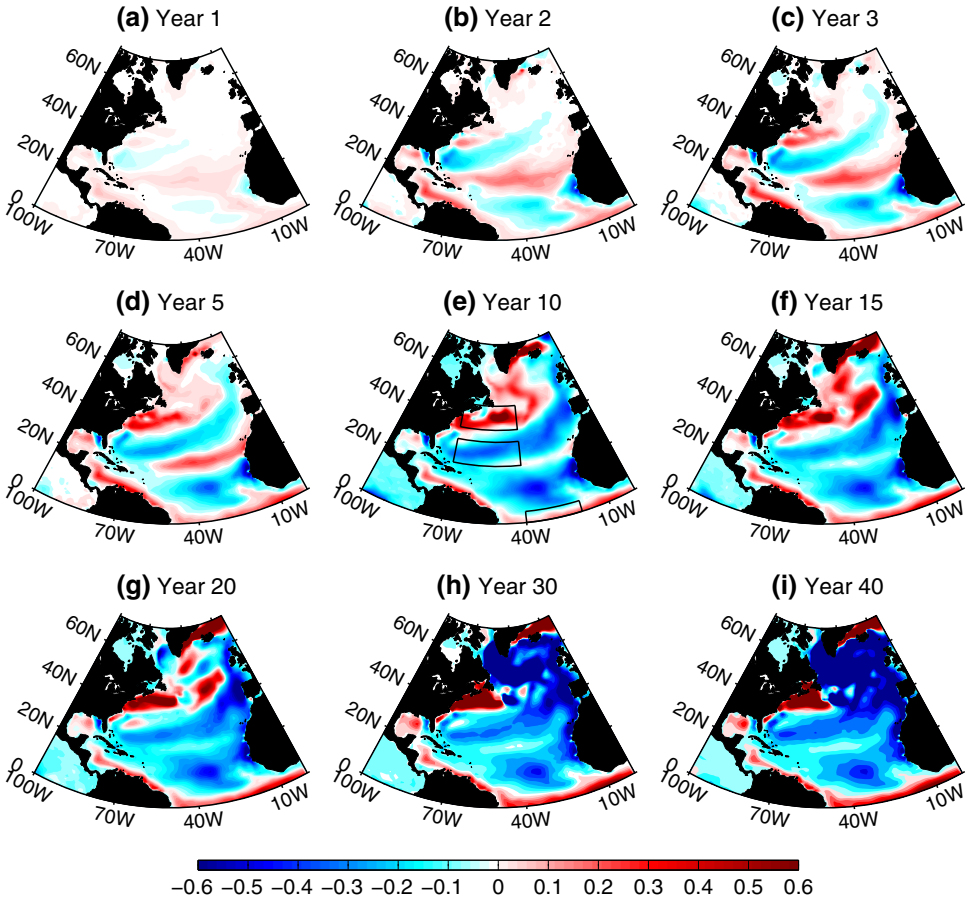

Fig. 10 Time evolution of sea surface temperature (0.1 °C) in 3AWP^{+} run in the first 40 years. The *black boxes* in **e** denote the regions performing the heat budget in Fig. 12d–f

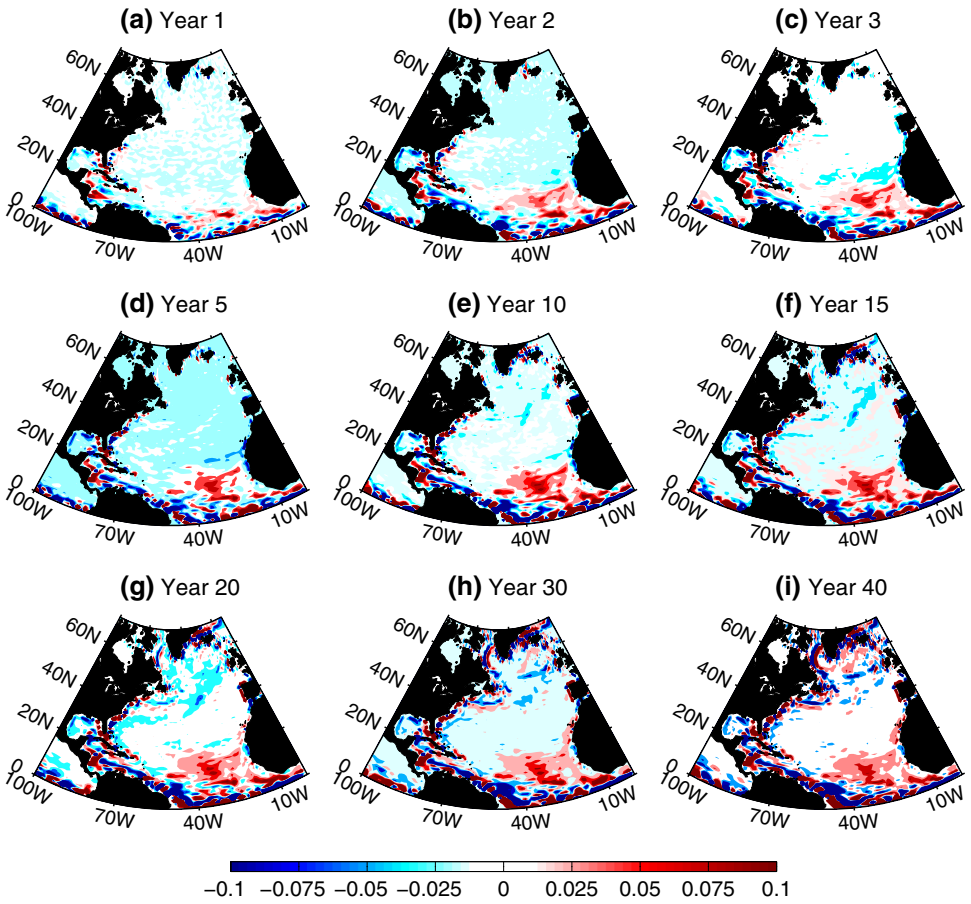

Fig. 11 Time evolution of vertical velocity (10^{-3} cm/s) at 50 m in 3AWP^{+} run in the first 40 years

The change of salinity significantly modulates the ocean circulation. In the upper ocean, the anomalous flow is characterized by anticyclonic gyres as a result of adjustments to the elevated SSH (Figs. 8, 9). In the first several years, there are mainly two anticyclonic gyre anomalies (Fig. 8a–d). One is located in the TNA, and the other is located in the region of the Gulf Stream. These circulation anomalies are a direct geostrophic response to the higher than normal SSH as a result of the seawater freshening, which is in agreement with previous studies (Zhang et al. 2011a, b, 2012; Zhang and Wu 2012). As more salt accumulated in the Gulf Stream and subtropical gyre region (Fig. 5e–i), the two separated anticyclonic gyre anomalies merge into one large gyre anomaly (Fig. 9a–d) and thus lead to a strengthening of the subtropical gyre. This basin-scale anticyclonic gyre anomaly strengthens the Gulf Stream and the recirculation. In addition, the boundary current anomalies are very distinct in our relatively high resolution ocean model compared to many low resolution climate models (e.g., Zhang et al. 2011a, b). In particular, it is interesting to note that the North Brazil current and south equatorial current (near the equator) are significantly weakened (Figs. 8, 9). As the anticyclonic gyre anomaly forms, a large amount of water is transported to the Caribbean Sea and Gulf Mexico by the southern branch of the anomalous gyre, which in turn generates a high sea level there. Due to the pressure gradient, the water flows out along the Brazil coast and further flows eastward along the equator.

4.1.3 Sea surface temperature response

The ocean current change eventually generates SST anomalies, as displayed in Fig. 10. While the SSS responses are quite uniform, the SST responses exhibit a complicated spatial pattern. The SST responses can be generally divided into three stages: local circulation induced warming and cooling anomalies (Fig. 10a–d), basin-scale gyre circulation induced warming and cooling responses (Fig. 10e–g) and the AMOC induced basin-scale SST changes (Fig. 10h, i). In the first stage, the North Atlantic SST anomaly is characterized by an alternating cold and warm temperature anomaly pattern, which is mainly trapped in the forcing region. This is because there are two local anticyclonic circulation responses to the initial freshwater forcing (Fig. 8a–d). The northern circulation locates in the western subtropics and tilts toward the northeast. The anomalous northeastward flow brings the

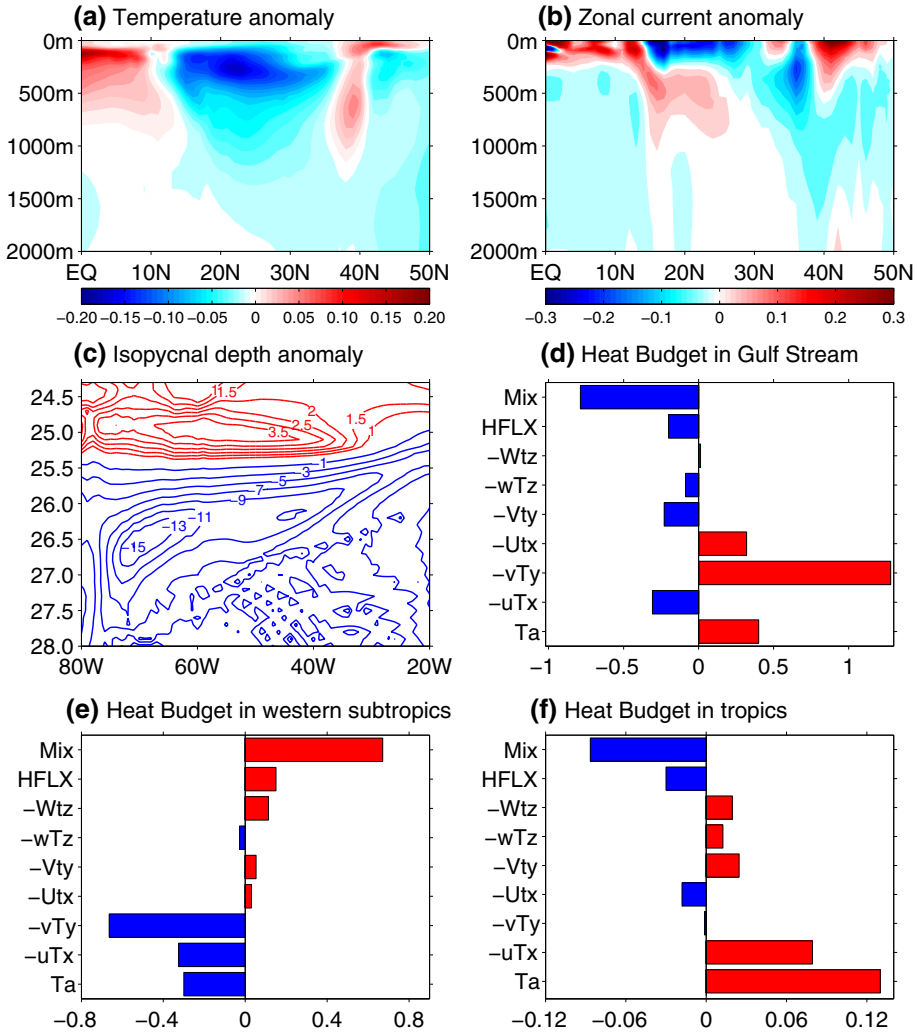

Fig. 12 Basin-scale gyre circulation response averaged between year 10 and year 20 in 3AWP^{+} run. Depth-latitude diagram for the Atlantic zonal mean **a** temperature and **b** zonal current responses. Positive means eastward. Units for the temperature and current are 0.1 °C and cm/s, respectively. **c** Density-longitude diagram of isopycnal depth averaged in a midlatitude belt (35°N–45°N). Unit is m. Heat budget in the **d** Gulf Stream, **e** western subtropics and **f** tropics (see three boxes in Fig. 10e) in 3AWP^{+} run. Ta (°C) denotes the SST anomalies averaged in the corresponding three *boxes*. Mix denotes the mixing and HFLX represents the surface heat flux forcing. The rest of the terms describe advection, with capital (U, V, W, T) and lower case (u, v, w, t) letters denoting mean and anomaly, respectively. −uTx, −vTy, −Utx, −Vty, −wTz and −Wtz represent term $-U'\partial\overline{T}/\partial x$, $-V'\partial\overline{T}/\partial y$, $-\overline{U}\partial T'/\partial x$, $-\overline{V}\partial T'/\partial y$, $-W'\partial\overline{T}/\partial z$and $-\overline{W}\partial T'/\partial z$, respectively. Unit for heat budget terms is 5×10^{-8} °C s^{-1}

warm subtropical water to the Gulf Stream region to generate warm anomalies, while the southwestward flow in the western subtropics brings cold subpolar water to the south to generate cold anomalies. Similarly, the local circulation anomaly in the TNA region generates a warming anomaly in the northern TNA ocean and a cooling anomaly in the southern TNA ocean. In addition to the southwestward cold advection, the cooling anomaly in the southern TNA ocean is also associated with the anomalous upwelling (Fig. 11). Here this anomalous upwelling is largely associated with the freshwater input. The positive freshwater anomaly can cause a decrease of density, a volume increase on sea water for given mass and thus a higher-than-normal SSH and an anomalous upwelling.

To demonstrate the dominant role of advection terms in the TNA cooling anomaly, we perform a time integrated heat budget over the TNA ocean. As shown in Fig. 6e and f, the mean temperature advection by the anomalous meridional current plays a dominant role and the advection by the anomalous zonal current is of secondary importance. The temperature advection by the upwelling also plays an important role in the TNA cooling anomaly. It is also found that the SST anomaly in the Gulf of Mexico, Caribbean Sea and the northern Brazil coast is mainly due to the upwelling and downwelling as shown in Fig. 11. As the two local anticyclonic circulations merge into one large basin-scale gyre into the next phase (Stage II), significant SST anomalies gradually extend to the entire ocean basin. Further examination finds that the SST response is featured by a north–south dipole, with a warming in the path of the Gulf Stream and NAC and a cooling to the south (Fig. 10e–g). At this stage, the SST dipole is apparently associated with the increased subtropical gyre (Fig. 9a–d), which will be focused in the next subsection. Note that the equatorial Atlantic Ocean is characterized by a warming anomaly (Fig. 10e–g). This warming mainly arises from the warm advection by the anomalous eastward current (Fig. 9a–d). After the 20th year (Stage III), the maximum SST anomaly shifts from the relatively low latitude to the high latitude (Fig. 10h, i). A tripole SST pattern in the North Atlantic

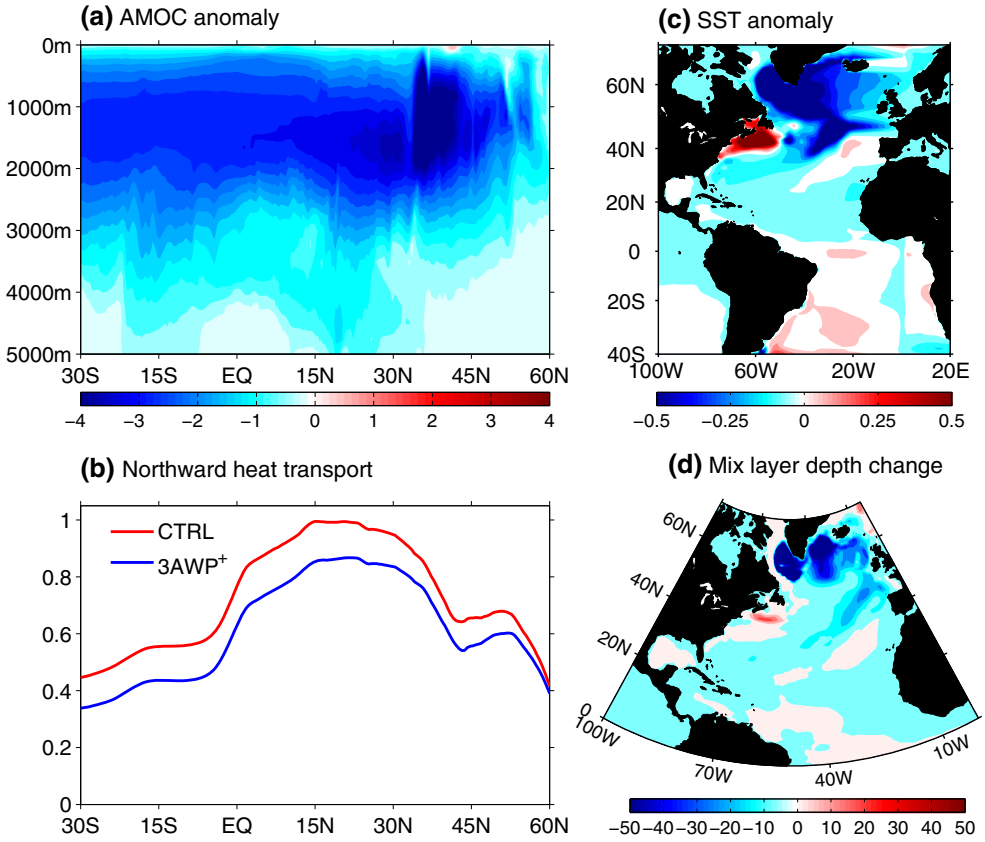

Fig. 13 Equilibrium ocean response in 3AWP^{+} run. **a** AMOC response (Sv). **b** Northward heat transport (PW). **c** SST response (°C). **d** Mixed layer depth response (m)

develops, with the largest amplitude over the subpolar regions. This SST response is similar to the cold phase of the AMO and also can be deemed as an SST response to the weakened AMOC. Since the AMOC gradually decreases during this stage (Fig. 4), we speculate that these SST anomalies are related to the AMOC changes, which will be discussed in the next section.

4.1.4 Basin-scale Gyre circulation adjustments

Based on the above analysis, we find that the multidecadal AWP-induced freshwater triggers a gyre circulation adjustment and then has the potential to affect the AMOC. This is because the salt flux takes time to be advected to the deep convection regions and the AMOC needs time to respond to salinity anomalies. Before the AMOC changes, ocean responses are dominated by the freshwater-induced gyre circulation adjustment particularly the basin-scale circulation adjustment.

To focus on the basin-scale gyre circulation adjustment, we average the ocean output from year 10 to year 20. Figure 12a displays the depth-latitude diagram for Atlantic zonal mean temperature anomaly. It is seen that the temperature anomaly in the subtropics and midlatitude can penetrate to about 1,500-m deep, but it is only trapped in the upper 600-m depth in the tropics, representing the north–south difference of vertical background mixing (strong deep convection in the high latitude versus relatively weak vertical mixing in the tropics). It is also found that the maximum temperature anomaly occurs in the subsurface rather than in the surface, implying that ocean dynamics dictate the temperature responses. The upper ocean anomalous anticyclonic circulation is also seen from the Atlantic zonal mean zonal velocity (Fig. 12b), with an anomalous eastward flow in the midlatitude and an anomalous westward flow in the subtropics. There is an exception around 36°N where anomalous westward flow exists. This appears to be linked to the recirculation. Associated with an acceleration of the subtropical gyre, the recirculation also strengthens, which in turn leads to a strengthened southwestward return flow around 36°N. Moreover, the tropical ocean is characterized by an anomalous eastward flow, which is consistent with that in Fig. 9a–d. Further inspection reveals that the lower layer circulation is opposite to the upper layer circulation, implying that the ocean circulation response to the AWP-induced freshwater is largely baroclinic (Fig. 12b), which is consistent with previous studies (e.g., Liu 1999). The

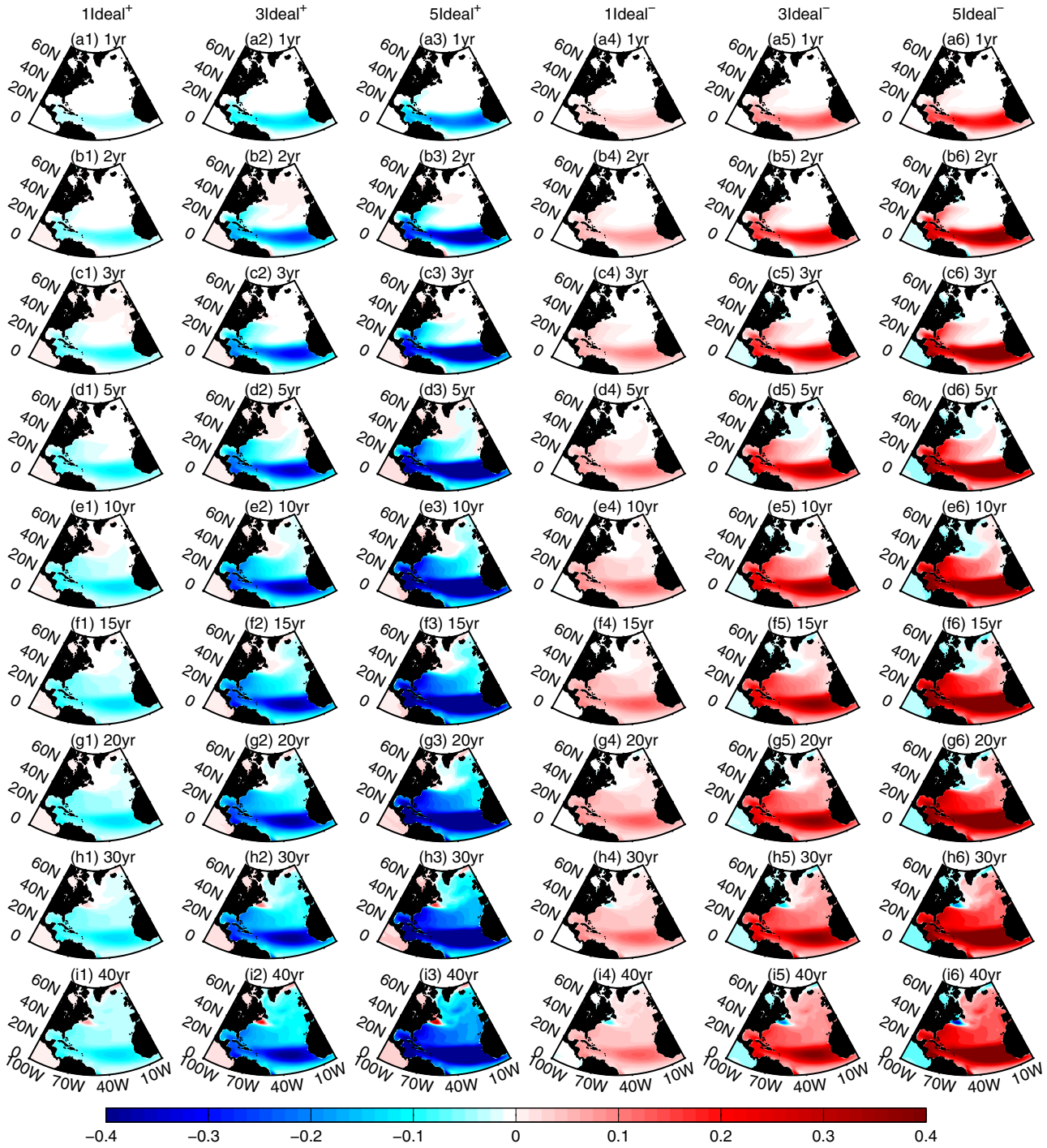

Fig. 14 Time evolution of sea surface salinity (PSU) response in *a1*–i1 1Ideal^{+}, *a2*–*i2* 3Ideal^{+}, *a3*–*i3* 5Ideal^{+}, *a4*–*i4* 1Ideal^{-}, *a5*–*i5* 3Ideal^{-}, and *a6*–*i6* 5Ideal^{-} runs in the first 40 years

ocean baroclinic response can be also seen in the changes of the isopycnal depths (Fig. 12c) which feature a deepening of the upper ocean pycnocline and a shoaling of the lower ocean pycnocline. Physically, a decrease of salinity leads to a decrease of density, a rising of surface water, and thus an increase of the SSH and a deepening (shoaling) of the upper (lower) ocean pycnocline.

To demonstrate the advection effect to the North Atlantic north–south temperature dipole, a mixed layer heat budget is conducted in the Gulf Stream region and the western subtropics denoted by the rectangular boxes in Fig. 10e, respectively (Fig. 12d, e). The heat budget analysis is based on the temperature conservation equation as follows:

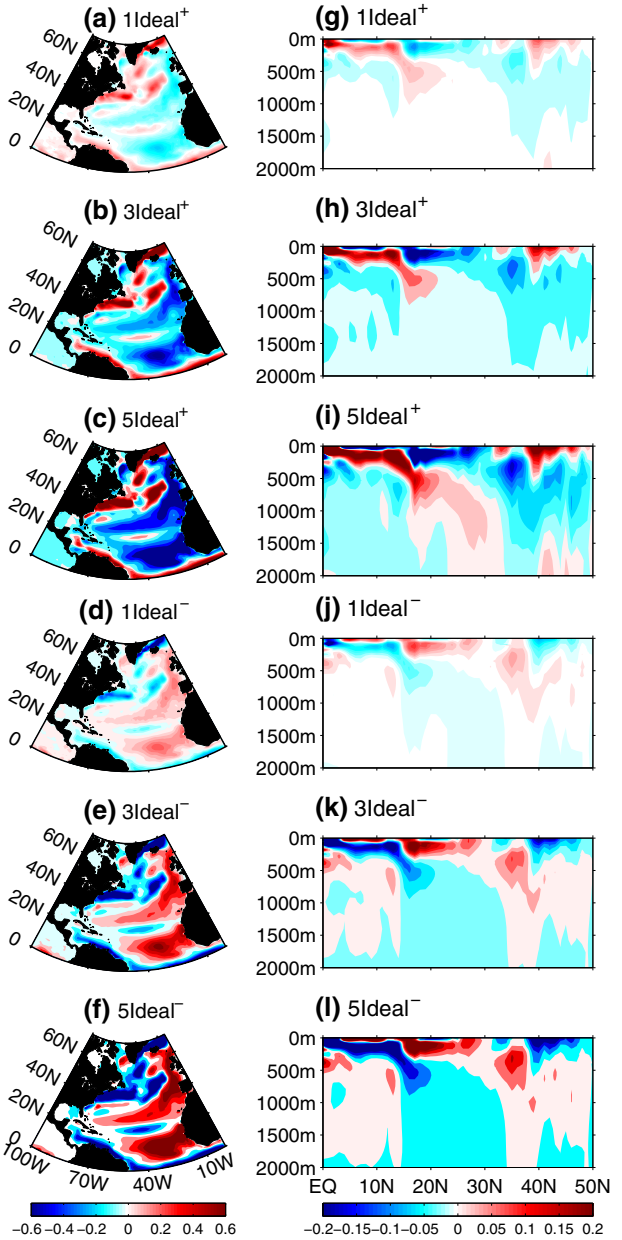

Fig. 15 Basin-scale gyre circulation response averaged between years 10 and 20 in 1Ideal$^+$, 3Ideal$^+$, 5Ideal$^+$, 1Ideal$^-$, 3Ideal$^-$, and 5Ideal$^-$ runs. **a**–**f** SST (0.1 °C) and **g**–**l** zonal mean zonal velocity (cm/s) averaged in the Atlantic basin

$$\frac{\partial T}{\partial t} = -u\frac{\partial T}{\partial x} - v\frac{\partial T}{\partial y} - w\frac{\partial T}{\partial z} + \frac{Q}{\rho C_p H} + Mix \qquad (2)$$

which includes, from left to right, local temperature change, advection, surface heat flux forcing and mixing term (estimated as the residual and including vertical entrainment, horizontal and vertical diffusions). The temperature equation is integrated in the mixed layer. Here, we choose the mixed layer depth as a constant (50 m). In the western subtropics (20°N–30°N, 70°W–40°W), the cooling is mainly associated with the anomalous meridional advection, and damped by heat flux and vertical mixing (Fig. 12e). The effect of advection by the anomalous zonal current is of secondary importance. In the Gulf Stream region (35°N–45°N, 70°W–40°W), the warming is largely associated with the anomalous meridional advection and countered by the heat flux and vertical mixing (Fig. 12d). The anomalous northeastward flow in the Gulf Stream region brings the warm subtropical water to the midlatitude to generate warm anomalies, while the southwestward flow in the central-eastern North Atlantic brings cold subpolar water to the western subtropics to generate warm anomalies. The strong vertical mixing in both regions acts to dilute the upper ocean anomalies down to the deeper ocean. We also perform a heat budget analysis in the tropical ocean (0°N–5°N, 40°W–20°W), as exhibited in Fig. 12f. As expected, the warming anomaly (Fig. 12a) is primarily dominated by the anomalous zonal advection, whereas the heat flux and mixing term play a damping role. Overall, the heat budget analysis is consistent with the ocean current response shown in Fig. 9. This further emphasizes the important contribution of ocean advection on the SST response during the gyre circulation adjustment stage.

4.2 Relative equilibrium response

In this section, we examine the ocean relative equilibrium response by focusing on the last 50-year of the 150-year model integration. The multidecadal AWP-induced freshwater influences the salinity and thus the density of the ocean surface water, which in turn affects the strength of the AMOC. Figure 13a displays the AMOC changes in 3AWP$^+$ run compared to that in the control simulation. The imposed negative salt flux weakens the AMOC by about 4 Sv, which accounts for 20 % of the mean transport (Fig. 1). The weakening of the AMOC also leads to a reduced poleward heat transport with the maximum decrease up to 15 % at 15°N (Fig. 13b). The weakened AMOC in 3AWP$^+$ run is primarily due to the weakening of North Atlantic deep convection as a result of negative salt flux input, which can be seen from the mixed layer depth change shown in Fig. 13d. The mixed layer depth significantly decreases in the North Atlantic Ocean, particularly in the deep convection region (the Irminger and Labrador Seas). As expected, the SST response to the AWP-induced freshening is characterized by an inter-hemispheric SST dipole over the Atlantic Ocean, with a cold SST anomaly in the North Atlantic and a slightly warm SST anomaly in the South Atlantic (Fig. 13c). In the North Atlantic, a tripole SST anomaly pattern develops, with the largest amplitude over the subpolar regions. These SST characteristics further indicate a weakening of the AMOC in 3AWP$^+$ run.

According to the results in the 3AWP$^+$ run, we conclude that the multidecadal AWP-induced freshwater

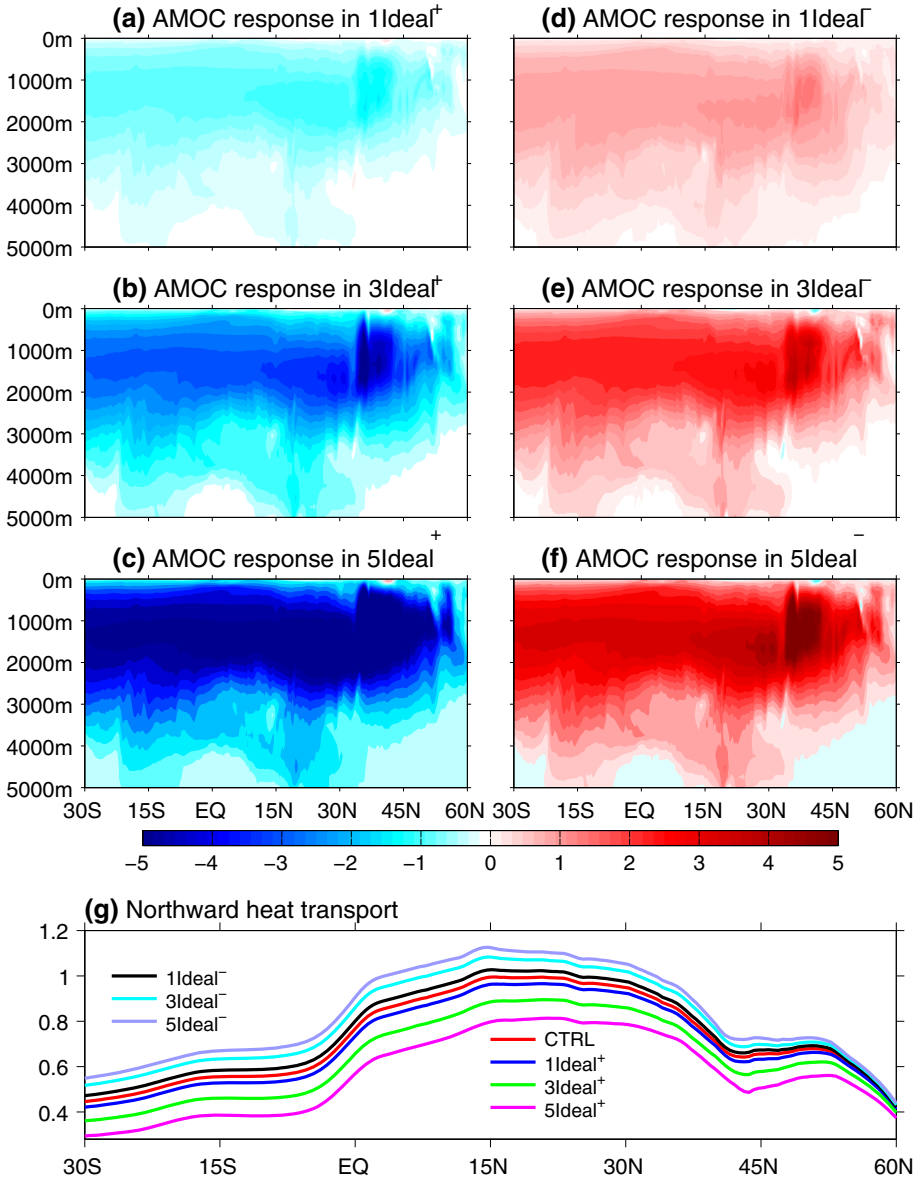

Fig. 16 Equilibrium AMOC (Sv) response in **a** 1Ideal^{+}, **b** 3Ideal^{+}, **c** 5Ideal^{+}, **d** 1Ideal^{-}, **e** 3Ideal^{-} and **f** 5Ideal^{-} runs. **g** Northward heat transport (PW) in control simulation and different freshwater forcing runs

flux has the potential to affect the AMOC, at least in the CESM1.0.4 ocean–sea ice model. With the multidecadal large AWP-induced freshwater forcing, the AMOC significantly decreases after about 30 years. It implies that the large AWP-induced freshwater flux plays a negative feedback role that acts to recover the AMOC after it is strengthened. That is, as the AMOC strengthens, its northward heat transport increases and thus the North Atlantic warms and the AWP become large. The large AWP increases rainfall in the TNA and decreases the cross-Central America moisture export to the eastern North Pacific (Wang et al. 2013). Both of these factors tend to increase freshwater and decrease salinity in the TNA. Advected northward by the ocean circulation, the negative salinity anomaly decreases the upper-ocean density in the deep water formation regions and thus weakens the AMOC.

5 Sensitivity to freshwater forcing amplitude and sign

To assess the sensitivity of ocean response to the amplitudes of low latitude freshwater forcing, six idealized experiments are conducted. The EmP forcing pattern shown in Fig. 3g and h are amplified one fold, threefold and fivefold and are named as 1Ideal^{+}, 3Ideal^{+}, 5Ideal^{+}, 1Ideal^{-}, 3Ideal^{-}, and 5Ideal^{-}, respectively.

The oceanic spin up process appears to be largely linear. As shown in Fig. 14a1–i3, the time evolution of negative SSS anomaly under the idealized positive freshwater

Table 1 AMOC (Sv) and northward heat transport (PW) responses at 26.5°N in the positive and negative idealized freshwater forcing runs

Variable	Year					
	20 year	50 year	80 year	100 year	120 year	150 year
AMOC (Sv)						
$5ideal^-$	0.5 (0.1)	3.5 (0.7)	4.8 (0.96)	5.2 (1.04)	4.7 (0.94)	3.8 (0.76)
$3ideal^-$	0.3 (0.1)	2.1 (0.7)	3.1 (1.03)	3.5 (1.17)	3.0 (1.0)	2.8 (0.93)
$1ideal^-$	0.1 (0.1)	0.7 (0.7)	1.0 (1.0)	1.0 (1.0)	1.05 (1.05)	1.0 (1.0)
$1ideal^+$	−0.1 (−0.1)	−0.7 (−0.7)	−1.0 (−1.0)	−1.05 (−1.05)	−1.08 (−1.08)	−1.1 (−1.1)
$3ideal^+$	−0.3 (−0.1)	−2.1 (−0.7)	−3.5 (−1.17)	−3.9 (−1.3)	−4.0 (−1.33)	−3.8 (−1.27)
$5ideal^+$	−0.5 (−0.1)	−3.5 (−0.7)	−5.8 (−1.16)	−6.7 (−1.34)	−7.1 (−1.42)	−7.5 (−1.5)
Heat transport (PW)						
$5ideal^-$	0.02 (0.004)	0.135 (0.027)	0.18 (0.036)	0.22 (0.044)	0.20 (0.04)	0.17 (0.035)
$3ideal^-$	0.012 (0.004)	0.084 (0.028)	0.12 (0.04)	0.15 (0.05)	0.11 (0.037)	0.10 (0.033)
$1ideal^-$	0.005 (0.004)	0.028 (0.028)	0.04 (0.04)	0.041 (0.041)	0.04 (0.04)	0.042 (0.042)
$1ideal^+$	−0.004 (−0.004)	−0.029 (−0.029)	−0.041 (−0.041)	−0.04 (−0.04)	−0.041 (−0.041)	−0.042 (−0.042)
$3ideal^+$	−0.0115 (−0.0038)	−0.082 (−0.027)	−0.14 (−0.047)	−0.16 (−0.053)	−0.17 (−0.0567)	−0.16 (−0.053)
$5ideal^+$	−0.02 (−0.004)	−0.14 (−0.028)	−0.22 (−0.044)	−0.23 (−0.046)	−0.25 (−0.05)	−0.26 (−0.052)

The values in the parentheses are normalized by the forcing values (per 1ideal fold)

forcing exerts a great similarity with that in $3AWP^+$ run (Fig. 5), albeit with a different magnitude. With the negative freshwater forcing in the TNA region, the direct response is a significant increase of SSS trapped in the forcing region (Fig. 14a4–a6). The positive SSS anomaly then spreads to the midlatitude by the Gulf Stream (Fig. 14b4–d6). In the following years, the positively salinity anomaly can be separated into two branches (Fig. 14e4–i6): one branch spreads northeastward, and thus joins the subpolar gyre and the other branch spreads southwestward and eventually joins the subtropical gyre. Overall, the amplitude of the salinity is linearly related to the freshwater forcing, with the freshwater amplified threefold (fivefold) coinciding with the salinity amplified threefold (fivefold). Moreover, the positive and negative freshwater induced salinity anomalies are quite antisymmetric. This indicates that the salinity spin up process is largely linear. The same is true for the anomalous SSH, ocean circulation, and temperature evolutions (not shown).

As expected, the basin-scale gyre circulation adjustment on decadal timescales is primarily a linear response (Fig. 15). Compared to the $3AWP^+$ run, the SST and circulation responses in $1Ideal^+$, $3Ideal^+$ and $5Ideal^+$ runs bear a similar spatial structure (Figs. 12a, b vs. 15a, b, c, g, h and i). For the negative freshwater forcing ($1Ideal^-$, $3Ideal^-$, and $5Ideal^-$), the SST response is mainly characterized by a dipole structure in the midlatitude, with a cooling in the Gulf Stream region and a warming in the subtropics (Fig. 15d–f). This dipole SST pattern is mainly driven by the salinity-induced anomalous cyclonic ocean circulation, which is largely baroclinic (Fig. 15j–l). The weakening of subtropical gyre and southern recirculation is also clearly seen (Fig. 15j–l). In general, the positive and negative freshwater forcing runs bear a similar spatial structure but with the opposite sign (Fig. 15a, b, c, g, h and i vs. d, e, f, j, k, and l).

Figure 16 shows the equilibrium AMOC response and its associated northward heat transport in different freshwater forcing runs. With the positive freshwater forcing, the AMOC and its corresponding northward heat transport are significantly decreased (Fig. 16a, b, c, and g). A close examination reveals that the AMOC decreases in $5Ideal^+$, $3Ideal^+$ and $1Ideal^+$ runs are not strictly linear, which can be also seen from the time evolution of the AMOC index displayed in Fig. 18. The ratio of AMOC decrease to freshwater magnitude is much larger in the $5Ideal^+$ run than that in the $3Ideal^+$ and $1Ideal^+$ runs, implying that the AMOC responses are sensitive to the amplitude of freshwater input.

The AMOC significantly increases in response to a negative freshwater forcing (Fig. 16d–f). The maximum AMOC streamfunction increases by 4.2, 3, and 1 Sv in the $5Ideal^-$, $3Ideal^-$ and $1Ideal^-$ runs, respectively (Fig. 18). Associated with the AMOC increase, the northward heat transport increases accordingly compared to the control simulation (Fig. 16g). Similar to the positive freshwater forcing runs, the AMOC is not linearly related to the magnitude of freshwater output. Moreover, although the low latitude freshwater forcing is exactly antisymmetric between the positive and negative freshwater forcing runs, the amplitude of the AMOC and its northward heat transport changes are not quite antisymmetric (Figs. 16, 18). One possible interpretation is that some important

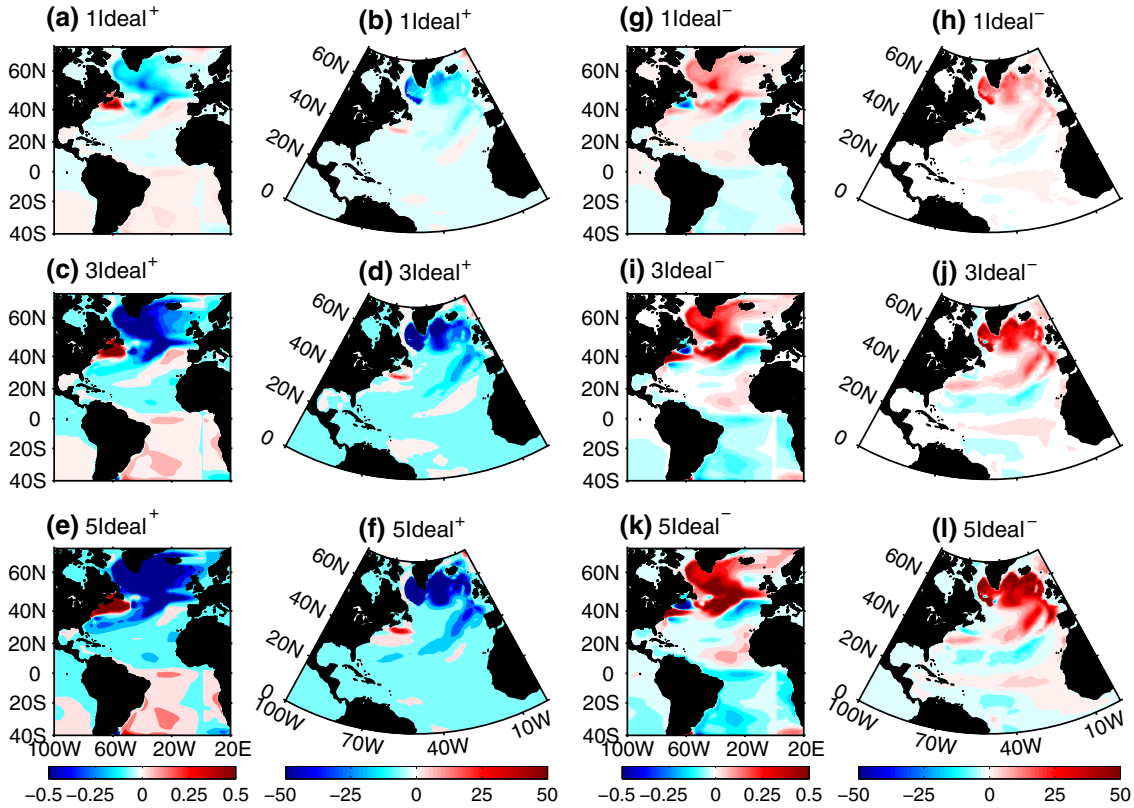

Fig. 17 Equilibrium SST (°C) and mixed layer depth (m) responses in **a**, **b** 1Ideal^{+}, **c**, **d** 3Ideal^{+}, **e**, **f** 5Ideal^{+}, **g**, **h** 1Ideal^{-}, **i**, **j** 3Ideal^{-} and **k**, **l** 5Ideal^{-} runs

processes involved in the AMOC response are nonlinear. However, it should be noted that the AMOC response is linear and symmetric before year 50, suggesting the transient response is linear that is different from the equilibrium response (Fig. 18). The same phenomena also occur at 26.5°N, as displayed in Table 1. It shows that the AMOC response during the spin up process (20 yr, 50 yr) is linear to the freshwater forcing. The maximum positive AMOC occurs at around 100 year and then decreases later for 5ideal^{-} and 3ideal^{-} cases. But it is not the true for 5ideal^{+} and 3ideal^{+} cases, which show still gradual decrease. Also the magnitude for 5ideal^{+}(3ideal^{+}) case is much higher than that of 5Ideal^{-} (3Ideal^{-}) case even at 100 year. Obviously, the AMOC is more sensitive to the low-latitude freshwater input than the low-latitude freshwater output. The northward heat transport response mainly follows the AMOC change. During the spin up process, the heat transport response is nearly linear. Similar to the AMOC response, the northward heat transport attains its peak at about 100 yr, and then decreases in the negative freshwater run (5ideal^{-}) and continues to increases in the positive freshwater run (5ideal^{+}). This suggests that the AMOC change plays a dominant role in northward heat transport change, whereas the contribution from horizontal gyre and temperature change is of secondary importance.

As expected, the low latitude salt flux change is eventually transported to the deep convection region, which generates a significant shoaling (deepening) of the mixed layer depth (Fig. 17b, d, f, h, j, and l) and thus decreases (increases) the AMOC strength. In response to the AMOC decrease (increase), the SST features an inter-hemispheric dipole seesaw (Fig. 17a, c, e, g, i and k), with a cooling (warming) in the north and a warming (cooling) in the south. Consistent with the AMOC response, the equilibrium mixed layer and SST responses are largely nonlinear in the positive and negative phases of the freshwater forcing runs.

6 Discussion and summary

Previous studies have suggested that, as the AMOC weakens, its northward heat transport reduces, thus the North Atlantic Ocean cools (the cold phase of the AMO) and the AWP becomes small. The opposite is true when the AMOC strengthens. Our recent analyses of observational data have indicated that the TNA region experiences a net freshwater gain (loss) during the multidecadal large (small) AWP period (Wang et al. 2013; Zhang and Wang 2012). Based on the observational analyses, Wang et al. (2013)

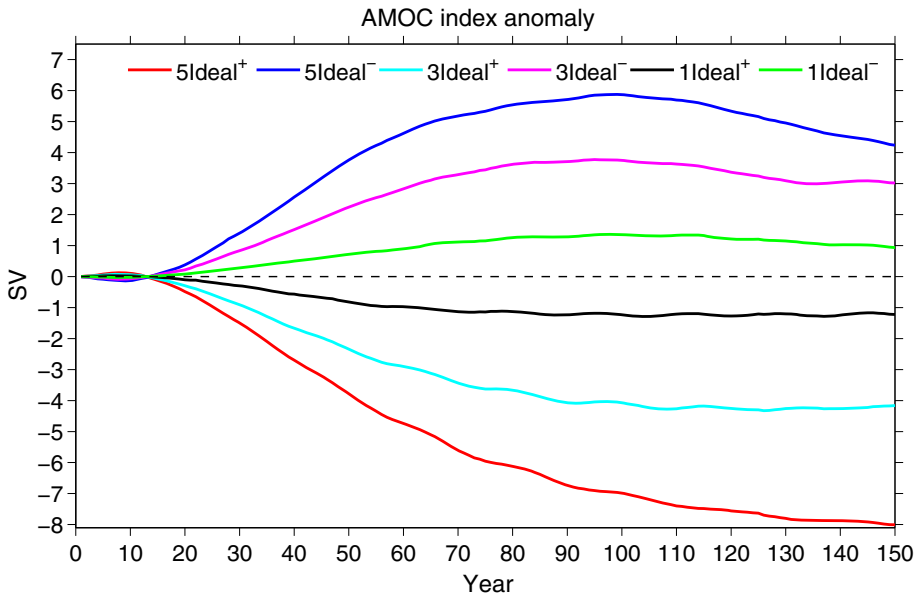

Fig. 18 Time evolution of the AMOC index for 6 experiments forced by the positive and negative idealized freshwater amplified fivefold (*red* and *dark blue lines*), threefold (*light blue* and *pink lines*) and onefold (*black* and *green lines*), respectively

hypothesized that the AWP-induced freshwater variability plays a negative feedback role that acts to recover the AMOC after it is weakened or strengthened. In the present paper, we test and confirm the hypothesis by using the ocean–sea ice model of CESM1.0.4 (Fig. 18).

Our model runs explicitly demonstrate that ocean response to the anomalous EmP forcing in the AWP region mainly includes two processes: Gyre circulation adjustments and the AMOC responses. For large AWPs, the negative EmP forcing directly forces a negative SSS anomaly. In the initial several years, the salinity anomalies are primarily trapped in the local TNA ocean and downstream of the Gulf Stream region. The salinity anomaly causes a decrease of density, a volume increase in sea water for given mass and thus a higher-than-normal SSH, which in turn sets up two local anticyclonic gyres as a result of the geostrophic adjustment, one located in the TNA ocean and the other in the western subtropics. Because of the advection by the anomalous anticyclonic gyre, particularly associated with the anomalous meridional current, the SST response is characterized by an alternating warming and cooling pattern in the western subtropical and tropical Atlantic Oceans. As time evolves, the salinity anomalies are further advected northeastward by the subpolar gyre and advected southwestward by the subtropical gyre. The salinity anomaly gradually reaches the deep convection region and more salt is accumulated in the subtropical gyre region. At this stage (about years 10–20), the two anticyclonic gyres merge into one large basin-scale gyre overlapping with the subtropical gyre. Therefore, this salinity-induced basin-scale circulation largely strengthens the Gulf Stream and the recirculation.

Accordingly, the SST response is featured by a dipole structure in the midlatitude and subtropics as a result of the anomalous meridional advection. As more and more salinity anomalies accumulated in the deep convection region advected by the Gulf Stream and subpolar gyre, the North Atlantic deep convection tends to be weakened, which eventually weakens the AMOC. After about the 30th year, a triple SST anomaly pattern in the North Atlantic Ocean develops, with the largest amplitude in the subpolar regions. This SST response is a characteristic of a weakened AMOC. When the system attains the equilibrium state, the ocean response is dominated by the AMOC change, which is characterized by a decreased northward heat transport and an inter-hemispheric SST seesaw. The opposite is true for the small AWP-induced freshwater forcing. Therefore, we conclude based on our model experiments that the multidecadal AWP-induced freshwater has the potential to affect the AMOC in such a way that the large (small) AWP-induced freshwater eventually leads to a weakening (strengthening) of the AMOC. It also indicates that the AWP-induced freshwater flux plays a negative feedback role that acts to recover the AMOC after it is weakened or strengthened, confirming the hypothesis inferred from observations by Wang et al. (2013).

The persistence time and amplitude of the AWP-induced freshwater flux are very important in affecting the AMOC, since the low latitudinal freshwater anomalies are diluted during their advection to the North Atlantic deep water formation regions. Thus, if the time span of the AWP-induced freshwater during the AMO warm (or cold) phase is longer than the advective time for surface waters to reach the North Atlantic, the deep water formation might be significantly disturbed. As demonstrated above, the AMOC

response to the AWP-induced freshwater change needs several decades to adjustment. This is because the freshwater advection to the deep convection region takes time and the AMOC response to the deep convection change may also require additional adjustment time (e.g., Lee and Wang 2010). Accompanied with the freshwater advection, a series gyre circulation adjustments occur. According to our model results, the AMOC significantly changes in response to the AWP-induced freshwater only after about the 30th year. In reality and most climate models, a half period of the AMO is about 30–35 years. That means the AWP-induced freshwater during the AMO's warm or cold phase can be persistent for 30–35 years. Therefore, our results suggest that the persistence of the AWP-induced freshwater during the AMO warm or cold phase is in favor of affecting the strength of the AMOC.

We also test the sensitivity of the AMOC response to the AWP-induced freshwater flux amplitude. In general, larger freshwater forcing induces larger AMOC amplitude response. However, the AMOC response to the freshwater forcing is not entirely linear. With the realistic AWP-induced freshwater forcing, the AMOC decreases or increases by about 1 Sv. When the AWP-induced freshwater forcing is amplified fivefold or threefold, the AMOC strength change increases substantially.

It seems that the AMOC change ($\sim$1 Sv) in response to a realistic AWP-induced freshwater forcing is a bit small. However, we should keep in mind that the AMOC's magnitude response can be highly model-dependent. The AMOC response to a certain freshwater forcing may be much larger in reality and other models. Here we only qualitatively rather than quantitatively assess the possibility of the AWP-induced freshwater forcing effect on the AMOC.

It is important to realize that, in a changing climate, the mean state of climate system can be shifted to a more AMO warm phase or a more AMO cold phase and thus the future freshwater forcing amplitude can be much larger than that used here. Therefore, the relationship between the multidecadal AWP-induced freshwater and the AMOC should be considered as a potentially important physical mechanism linking tropical and high-latitude climate in context of past and future climate changes. Another point is that here we only use an ocean–sea ice model in which air–sea feedbacks are eliminated. The AMOC change may be amplified or damped under the air–sea feedbacks in the coupled ocean–atmosphere system. A further study of the interactions among the AMOC, AMO and AWP is needed by using fully coupled ocean–atmosphere models, which is our next step of research.

Although our study here only focuses on the role of multidecadal time scale freshwater on the AMOC, the finding can also be applicable to longer time scale response, e.g., centennial or longer. Our mechanisms here are consistent with that in Vellinga and Wu (2004) who describe a centennial variability in a control simulation. This suggests that the physical mechanism of low-latitude freshwater on the AMOC is not very sensitive to the freshwater forcing period. This indication can be also seen in Park and Latif (2012). By analyzing idealized forced simulations, they show that the spatial structure of the forcing is important rather than its period, of which forcing is somewhat similar to AWP-related freshwater anomalies in the present work.

Acknowledgments This work was supported by grants from National Oceanic and Atmospheric Administration (NOAA) Climate Program Office and the base funding of NOAA Atlantic Oceanographic and Meteorological Laboratory (AOML). The findings and conclusions in this report are those of the author(s) and do not necessarily represent the views of the funding agency.

References

Bell GD, Chelliah M (2006) Leading tropical modes associated with interannual and multidecadal fluctuations in north Atlantic hurricane activity. J Clim 19:590–612

Clement AC, Peterson LC (2008) Mechanisms of abrupt climate change of the last glacial period. Rev Geophys 46:RG4002. doi:10.1029/2006RG000204

Compo GP et al (2011) The twentieth century reanalysis project. Q J R Meteorol Soc 137:1–28

Danabasoglu G, Bates SC, Briegleb BP, Jayne SR, Jochum M, Large WG, Peacock Synte, Yeager SG (2012) The CCSM4 ocean component. J Clim 25:1361–1389

Delworth TL, Mann ME (2000) Observed and simulated multidecadal variability in the Northern Hemisphere. Clim Dyn 16:661–676

Delworth TL, Manabe S, Stouffer RJ (1993) Interdecadal variation in the thermohaline circulation in a coupled ocean atmosphere model. J Clim 6:1993–2011

Deshayes J, Frankignoul C (2008) Simulated variability of the circulation of the North Atlantic from 1953 to 2003. J Clim 21:4919–4933

Dickson R, Lazier J, Meincke J, Rhines P, Swift J (1996) Long term coordinated changes in the convective activity of the North Atlantic. Prog Oceanogr 38:241–295

Dijkstra HA, Te Raa LA, Schmeits M, Gerrits J (2006) On the physics of the Atlantic multidecadal oscillation. Ocean Dyn 56:36–50

Dong BW, Sutton RT (2002) Adjustment of the coupled ocean–atmosphere system to a sudden change in the thermohaline circulation. Geophys Res Lett 29:1728. doi:10.1029/2002GL015229

Eden C, Willebrand J (2001) Mechanisms of interannual to decadal variability of the North Atlantic circulation. J Clim 14: 2266–2280

Enfield DB, Lee SK (2005) The heat balance of the Western Hemisphere warm pool. J Clim 18:2662–2681

Enfield DB, Mestas-Nunez AM, Trimble PJ (2001) The Atlantic multidecadal oscillation and its relationship to rainfall and river flows in the continental US. Geophys Res Lett 28:2077–2080

Ganachaud A, Wunsch C (2000) Improved estimates of global ocean circulation, heat transport and mixing from hydrological data. Nature 408:453–457

Goldenberg SB, Landsea C, Mestas-Nunez AM, Gray WM (2001) The recent increase in Atlantic hurricane activity. Science 293:474–479

Häkkinen S (1999) Variability of the simulated meridional heat transport in the North Atlantic for the period 1951–1993. J Geophys Res 104:10991–11007
Huang B, Mehta VM (2004) Response of the Indo-Pacific warm pool to interannual variations in net atmospheric freshwater. J Geophys Res 109:C06022. doi:10.1029/2003JC002114
Huang B, Mehta VM (2005) Response of the Pacific and Atlantic Oceans to interannual variations in net atmospheric freshwater. J Geophys Res 110:C08008. doi:10.1029/2004JC002830
Huang B, Mehta VM, Schneider N (2005) Oceanic response to idealized net atmospheric freshwater in the Pacific at the decadal time scale. J Phys Oceanogr 35:2467–2486
Kanzow T et al (2010) Seasonal variability of the Atlantic meridional overturning circulation at 26.5°N. J Clim 23:5678–5698
Knight JR et al (2005) A signature of persistent natural thermohaline circulation cycles in observed climate. Geophys Res Lett 32. doi:10.1029/2005GL024233
Krebs U, Timmermann A (2007a) Fast advective recovery of the Atlantic meridional overturning circulation after a Heinrich event. Paleoceanography 22. doi:10.1029/2005PA001259
Krebs U, Timmermann A (2007b) Tropical air–sea interactions accelerate the recovery of the Atlantic Meridional overturning circulation after a major shutdown. J Climate 20:4940–4956
Large WG, Yeager SG (2009) The global climatology of an interannually varying air–sea flux data set. Clim Dyn 33: 341–364
Lavender KL, Davis RE, Owens WB (2002) Observations of open-ocean deep convection in the Labrador Sea from subsurface floats. J Phys Oceanogr 32:511–526
Lee SK, Wang C (2010) Delayed advective oscillation of the Atlantic thermohaline circulation. J Clim 23:1254–1261
Lee SK, Enfield DB, Wang C (2007) What drives seasonal onset and decay of the Western Hemisphere warm pool? J Clim 20:2133–2146
Liu Z (1999) Forced planetary wave response in a thermocline gyre. J Phys Oceanogr 29:1036–1055
Lumpkin R, Speer K (2007) Global ocean meridional overturning. J Phys Oceanogr 37:2550–2562
Manabe S, Stouffer RJ (1995) Simulation of abrupt climate change induced by freshwater input to the North Atlantic ocean. Nature 378:165–167
Manabe S, Stouffer RJ (1999a) The role of thermohaline circulation in climate. Tellus 51A:91–109
Manabe S, Stouffer RJ (1999b) Are two modes of thermohaline circulation stable? Tellus 51A:400–411
McCabe G, Palecki M, Betancourt J (2004) Pacific and Atlantic Ocean influences on multidecadal drought frequency in the United States. Proc Nat Acad Sci 101:4136–4141
Medhaug I, Furevik T (2011) North Atlantic 20th century multidecadal variability in coupled climate models: sea surface temperature and ocean overturning circulation. Ocean Sci Discuss 8:353–396
Medhaug I, Langehaug HR, Eldevik T, Furevik T, Bentsen M (2012) Mechanisms for decadal scale variability in a simulated Atlantic meridional overturning circulation. Clim Dyn 39:77–93
Msadek R, Frankignoul C (2009) Atlantic multidecadal oceanic variability and its influence on the atmosphere in a climate model. Clim Dyn 33:45–62
Okumura Y, Deser C, Hu A, Timmerman A, Xie S (2009) North Pacific climate response to freshwater forcing in the Subartic North Atlantic: ocean and atmospheric pathways. J Clim 22:1424–1445
Park W, Latif M (2012) Atlantic meridional overturning circulation response to idealized external forcing. Clim Dyn 39:1709–1726. doi:10.1007/s00382-011-1212-0
Pickart RS, Spall MA, Ribergaard MH, Moore GWK, Milliff RF (2002) Deep convection in the Irminger sea forced by the Greenland tip jet. Nature 424:152–156
Smith TM, Reynolds RW, Peterson TC, Lawrimore J (2008) Improvements to NOAA's Historical Merged Land-Ocean Surface Temperature Analysis (1880–2006). J Clim 21:2283–2296
Stouffer RJ, Seidov D, Haupt BJ (2007) Climate response to external sources of freshwater: North Atlantic versus the Southern Ocean. J. Climate 20:436–448
te Raa LA, Dijkstra HA (2002) Instability of the thermohaline ocean circulation on interdecadal timescales. J Phys Oceanogr 32:138–160
Timmermann A, An S, Krebs U, Goosse H (2005) ENSO suppression due to a weakening of the North Atlantic thermohaline circulation. J Clim 18:3122–3139
Vellinga M, Wu P (2004) Low-latitude freshwater influence on centennial variability of the Atlantic thermohaline circulation. J Clim 17:4498–4511
Wang C, Enfield DB (2001) The tropical Western Hemisphere warm pool. Geophys Res Lett 28:1635–1638
Wang C, Enfield DB (2003) A further study of the tropical Western Hemisphere warm pool. J Clim 16:1476–1493
Wang C, Lee SK (2009) Co-variability of tropical cyclones in the North Atlantic and the eastern North Pacific. Geophy Res Lett 36:L24702. doi:10.1029/2009GL041469
Wang C, Zhang L (2013) Multidecadal ocean temperature and salinity variability in the tropical North Atlantic: linking with the AMO, AMOC and subtropical cell. J Clim (in press)
Wang C, Lee SK, Enfield DB (2008a) Climate response to anomalously large and small Atlantic warm pools during the summer. J Clim 21:2437–2450
Wang C, Lee SK, Enfield DB (2008b) Atlantic warm pool acting as a link between Atlantic multidecadal oscillation and Atlantic tropical cyclone activity. Geochem Geophys Geosyst 9:Q05V03. doi:10.1029/2007GC001809
Wang C, Liu H, Lee SK, Atlas R (2011) Impact of the Atlantic warm pool on United States landfalling hurricanes. Geophys Res Let. doi:10.1029/2011GL049265
Wang C, Zhang L, Lee SK (2013) Response of freshwater flux and sea surface salinity to variability of the Atlantic warm pool. J Clim 26:1249–1267
Wu L, Li C, Yang C, Xie SP (2008) Global teleconnections in response to a shutdown of the Atlantic meridional overturning circulation. J Clim 21:3002–3019
Zhang R-H, Busalacchi AJ (2009) Freshwater Flux (FWF)-Induced Oceanic feedback in a hybrid coupled model of the tropical Pacific. J Climate 22:853–879
Zhang R, Delworth T (2005) Simulated tropical response to a substantial weakening of the Atlantic thermohaline circulation. J Clim 18:1853–1860
Zhang L, Wang C (2012) Remote influences on freshwater flux variability in the Atlantic warm pool region. Geophys Res Lett 39:L19714. doi:10.1029/2012GL053530
Zhang L, Wu L (2012) Can oceanic freshwater flux amplify global warming? J Clim 25:3417–3430
Zhang R, Delworth TL, Held IM (2007) Can the Atlantic Ocean drive the observed multidecadal variability in Northern Hemisphere mean temperature? Geophys Res Lett 34:L02709. doi:10.1029/2006GL028683
Zhang L, Wu L, Zhang J (2011a) Coupled ocean-atmosphere responses to recent freshwater flux changes over the Kuroshio-Oyashio extension region. J Clim 24:1507–1524
Zhang L, Wu L, Zhang J (2011b) Simulated response to recent freshwater flux change over the gulf stream and its extension:

coupled Ocean-Atmosphere adjustment and Atlantic-Pacific Teleconnection. J Clim 24:3971–3988

Zhang R-H, Zheng F, Zhu JS, Pei YH, Zheng Q, Wang ZG (2012) Modulation of El Niño-Southern Oscillation by freshwater flux and salinity variability in the tropical Pacific. Adv Atmos Sci 29(4):647–660

Zhang R-H, Zheng F, Zhu J, Wang Z (2013) A successful real-time forecast of the 2010–11 La Niña event. Sci Rep 3:1108